REPORT DOCUMENTATION PAGE

Form Approved OMB NO. 0704-0188

1. REPORT DATE (DD-MM-YYYY)	2. REPORT TYPE	3. DATES COVERED (From - To)
29-04-2011	Final Report	1-May-2008 - 30-Apr-2011

4. TITLE AND SUBTITLE	5a. CONTRACT NUMBER
Piezoelectric Pulsed Microjets Final Report	W911NF-08-1-0100
	5b. GRANT NUMBER
	5c. PROGRAM ELEMENT NUMBER
	611102

6. AUTHORS	5d. PROJECT NUMBER
William S. Oates, Farrukh Alvi	
	5e. TASK NUMBER
	5f. WORK UNIT NUMBER

7. PERFORMING ORGANIZATION NAMES AND ADDRESSES	8. PERFORMING ORGANIZATION REPORT NUMBER
Florida State University Sponsored Research Services Florida State University Tallahassee, FL 32306 -4166	

9. SPONSORING/MONITORING AGENCY NAME(S) AND ADDRESS(ES)	10. SPONSOR/MONITOR'S ACRONYM(S)
U.S. Army Research Office P.O. Box 12211 Research Triangle Park, NC 27709-2211	ARO
	11. SPONSOR/MONITOR'S REPORT NUMBER(S)
	53264-EG.3

12. DISTRIBUTION AVAILIBILITY STATEMENT

Approved for Public Release; Distribution Unlimited

13. SUPPLEMENTARY NOTES

The views, opinions and/or findings contained in this report are those of the author(s) and should not contrued as an official Department of the Army position, policy or decision, unless so designated by other documentation.

14. ABSTRACT

This reports summarizes an investigation of coupling broadband piezoelectric actuators with large force microjet actuators to achieve pulsed flow control over a broad frequency range. The development is relevant to a range of flow control problems for rotorcraft noise control and dynamic stall, jet inlet flow separation, cavity bay flow control, etc. The results have provided multi-physics modeling describing the actuator dynamics, high fidelity aero-acoustic computations, and smart structure and fluid dynamic experimental characterization. It is shown that

15. SUBJECT TERMS

microjets, piezoelectric actuators, flow control, broadband actuation

16. SECURITY CLASSIFICATION OF:			17. LIMITATION OF ABSTRACT	15. NUMBER OF PAGES	19a. NAME OF RESPONSIBLE PERSON
a. REPORT	b. ABSTRACT	c. THIS PAGE	UU		William Oates
UU	UU	UU			19b. TELEPHONE NUMBER
					850-410-6190

Report Title

Piezoelectric Pulsed Microjets Final Report

ABSTRACT

This reports summarizes an investigation of coupling broadband piezoelectric actuators with large force microjet actuators to achieve pulsed flow control over a broad frequency range. The development is relevant to a range of flow control problems for rotorcraft noise control and dynamic stall, jet inlet flow separation, cavity bay flow control, etc. The results have provided multi-physics modeling describing the actuator dynamics, high fidelity aero-acoustic computations, and smart structure and fluid dynamic experimental characterization. It is shown that the piezoelectric actuator achieved pulsed flow actuation from quasi-static up to at least 1.6kHz. Pulsed supersonic microjet flow was confirmed using micro-schlieren imagery up to 800Hz. The first design was also extended to a highly compact microjet actuator capable of comparable pulsed actuation which is expected to facilitate technology transfer.

List of papers submitted or published that acknowledge ARO support during this reporting period. List the papers, including journal references, in the following categories:

(a) Papers published in peer-reviewed journals (N/A for none)

Number of Papers published in peer-reviewed journals: 0.00

(b) Papers published in non-peer-reviewed journals or in conference proceedings (N/A for none)

Number of Papers published in non peer-reviewed journals: 0.00

(c) Presentations

Hogue, J., "Broadband Microjet Flow Control Using Piezoelectric Actuators," Master's Thesis, Florida State University, 2011.

Number of Presentations: 1.00

Non Peer-Reviewed Conference Proceeding publications (other than abstracts):

Number of Non Peer-Reviewed Conference Proceeding publications (other than abstracts):   0

Peer-Reviewed Conference Proceeding publications (other than abstracts):

Number of Peer-Reviewed Conference Proceeding publications (other than abstracts):   0

(d) Manuscripts

Hogue, J., Kumar, R., Alvi, F., Oates, W., "Experimental Characterization of Broad Bandwidth Piezohydraulic Microjets", to be submitted to J. Mater. Syst. Struct.

Number of Manuscripts: 1.00

Patents Submitted

13/069,872 High Frequency Pulsed Microjet Actuation

Patents Awarded

Awards

Graduate Students

NAME	PERCENT_SUPPORTED
Joshua Hogue	1.00
FTE Equivalent:	**1.00**
Total Number:	**1**

Names of Post Doctorates

NAME	PERCENT_SUPPORTED
Ali Uzun	0.50
FTE Equivalent:	**0.50**
Total Number:	**1**

Names of Faculty Supported

NAME	PERCENT_SUPPORTED	National Academy Member
W. Oates	0.50	No
F. Alvi	0.50	No
FTE Equivalent:	**1.00**	
Total Number:	**2**	

Names of Under Graduate students supported

NAME	PERCENT_SUPPORTED
FTE Equivalent:	
Total Number:	

Student Metrics
This section only applies to graduating undergraduates supported by this agreement in this reporting period

The number of undergraduates funded by this agreement who graduated during this period: 0.00

The number of undergraduates funded by this agreement who graduated during this period with a degree in science, mathematics, engineering, or technology fields:...... 0.00

The number of undergraduates funded by your agreement who graduated during this period and will continue to pursue a graduate or Ph.D. degree in science, mathematics, engineering, or technology fields:...... 0.00

Number of graduating undergraduates who achieved a 3.5 GPA to 4.0 (4.0 max scale):...... 0.00

Number of graduating undergraduates funded by a DoD funded Center of Excellence grant for Education, Research and Engineering:...... 0.00

The number of undergraduates funded by your agreement who graduated during this period and intend to work for the Department of Defense 0.00

The number of undergraduates funded by your agreement who graduated during this period and will receive scholarships or fellowships for further studies in science, mathematics, engineering or technology fields: 0.00

Names of Personnel receiving masters degrees

NAME

Fei Liu

Joshua Hogue

Total Number: **2**

Names of personnel receiving PHDs

NAME

Total Number:

Names of other research staff

NAME   PERCENT_SUPPORTED

FTE Equivalent:

Total Number:

Sub Contractors (DD882)

Inventions (DD882)

5   High Frequency Pulsed Microjet Actuation

Patent Filed in US? (5d-1)   Y

Patent Filed in Foreign Countries? (5d-2)   N

Was the assignment forwarded to the contracting officer? (5e)   N

Foreign Countries of application (5g-2):

    5a: William S. Oates

5f-1a: Florida State University

  5f-c: 2525 Pottsdamer St.

    Tallahassee   FL   32310

    5a: Jonathan Clark

5f-1a: Florida State University

  5f-c: 2525 Pottsdamer St.

    Tallahassee   FL   32310

    5a: Farrukh Alvi

5f-1a: Florida State University

  5f-c: 2525 Pottsdamer St.

    Tallahassee   FL   32310

Scientific Progress

A set of new microjet actuators were designed, tested, and modeled which show dramatic increases in flow control capabilities. The piezohydraulic actuator is capable of pulsing air through a microjet from 0 to >1 Mach at frequencies from quasi-static to 1.6kHz(the fastest known for microjet actuators).

A resonanced enhanced actuator was designed, tested, and modeled to understand how active structures can be used to pulse flow in an ultra-compact actuator system. High fidelity aero-acoustic CFD modeling was used to understand how the internal pulsed flow interacts with the cavity structure.

A piezoelectric supersonic nozzle was designed and tested as the next generation in broadband pulsed flow. This system significantly reduces the size and reliability issues of the piezohydraulic system. This is achieved through direct flow amplification by deforming the nozzle of a converging-diverging nozzle. Supersonic flow and direct visualization of the nozzle deformation were measured. A patent was submitted on this invention.

Technology Transfer

Broadband Microjet Flow Control Using Piezoelectric Actuators

PI: William S. Oates * co-PI: Farrukh Alvi [†]

Florida Center for Advanced Aero Propulsion (FCAAP)[*,†]
Department of Mechanical Engineering
Florida A & M and Florida State University
Tallahassee, FL 32310

[*]Email: woates@eng.fsu.edu, Telephone: (850) 410-6190
[†]Email: alvi@eng.fsu.edu, Telephone: (850) 644-0053

Contents

Abstract

This project summarizes an investigation of advanced, broadband microjet actuators that can achieve pulsed *supersonic* flow over a frequency range of quasi-steady to 1-10 kHz. The project was interdisciplinary in nature which combined research in solid mechanics and actuator development of novel smart structures with advanced flow control concepts and flow visualization diagnostics. In particular to this study, a piezohydraulic microjet flow control actuator was designed, modeled and experimentally characterized to enhance the capabilities for flow separation control and noise reduction on aircraft control surfaces such as rotorcraft. A summary of the design of the piezohydraulic microjet, system dynamic modeling, and experimental results are presented that demonstrate broadband flow characteristics. The results predominantly focus on a microjet actuator that is coupled to a piezoelectric stack actuator and a hydraulic circuit to amplify the stack actuator displacement and in turn, throttle flow through the microjet. The system dynamic modeling illustrates how key internal mechanisms contribute to significantly large displacement amplication that is achievable at relatively high frequencies ($\sim$1.6 kHz and potentially greater). The actuator dynamics are compared to quantitative unsteady pressure measurements at the microjet exit and high-speed micro-Schlieren imagery to quantify the exit flow field under pulsed flow actuation. The results illustrate broadband *supersonic* pulsed microjet actuator performance using the piezohydraulic circuit. In additional to the piezohydraulic actuator results, the final section presents preliminary developments on next generation actuators that build upon the piezohydraulic design. Two actuators are presented that are significantly smaller in size and weight, more reliable, and exhibit comparable, broadband pulsed flow actuation.

1 INTRODUCTION

The ability to actively control high speed aerodynamic flow provides many challenges and opportunities to rectify adverse flow separation that occurs with high performance aircraft. Early boundary-layer flow research focused on the goal of laminar-flow control to improve aircraft fuel consumption and range [1]. Much has changed from research on boundary-layer control in the early 1900's to the present day research which has transitioned to steady mass injection or more advanced high-frequency pulsed flow interactions with boundary-layer flow. Recent research in this area has focused on various active and passive control methods to manipulate flow separation and suppress acoustic resonance to increase aircraft performance and maneuverability. Non-passive alterations to the boundary layer flow of structures such as airfoils, compressor blades, or cavity flows have created unique opportunities to improve aerodynamic performance dependent upon the surrounding environmental conditions or the oscillatory nature of mechanical devices like rotor blades [2]. To enhance the effects of boundary layer control, the need for broadband actuation is critical to achieve robustness and enhanced agility over a broader operating regime. The combination of smart materials exhibiting high frequency response characteristics and modern microjet applications provide a viable alternative to address this active flow control challenge.

Pulsed flow systems have received an increase in attention in recent years due to the opportunities for substantial gain in performance when adding the ability to actively control this flow. Boundary-layer control has evolved immensely from early suction flow control, tested first by Prandt in the 1930's, to steady flow control implemented by blowing air across flap surfaces for separation delay in the 1950's [3]. Passive flow control techniques such as vortex generators, riblets, and strakes have also since been implemented to enhance flow re-attachment [4–6]. However, passive techniques often produce unwanted drag in certain ambient flow conditions and lack the adaptability relative to many active flow control techniques.

In the past couple of decades, research on boundary-layer flow control has significantly increased in the area of active flow control relative to passive methods. Active control of boundary layer flow

has predominantly focused on steady and unsteady methods that increase robustness for mitigating undesirable flow conditions. Active methods that use an external energy source to input energy into the flow can be categorized into either steady mass flow, pulsed mass flow, or zero net mass flow systems. Steady mass flow and pulsed mass flow systems are associated with a nonzero mass addition to the boundary layer [7]. These systems are characteristic of requiring a reservoir pressure source to supply the energy input into the flow for manipulation of the inherent behavior of shear or boundary layer flow. Steady flow systems, such as supersonic steady flow microjets, have been experimentally shown to reduce noise and interrupt adverse flow structures [8–10]. Zero net mass flow systems, such as synthetic jets and "SparkJet" systems, produce no net mass flow while maintaining a net momentum flux [11, 12].

Despite the idea that an active means of flow control is superior to a passive means, active flow control varies greatly in its performance attributes. The question often arises, which means of active flow control is preferred; steady or unsteady pulsed flow? When the attributes of power consumption and, in some situations, system complexity are investigated, unsteady flow is often concluded to be superior to constant mass-injection flow schemes [3]. The addition of a periodic or controllable input to active control has become the predominate goal in current flow control research. Active systems can further be grouped with either open or closed loop control. An open loop control scheme inherently requires no feedback signal compared to closed loop control which depends on a transient feedback and advanced aero-acoustic or fluid-structure control algorithms [13]. The combination of closed loop control and active pulsed flow presents opportunities to vary the net mass and momentum added to the overall system along with reducing the power required for system operation. However, known issues of pulsed flow actuators have included limited actuation forces and bandwidth due to power limitations and a lack of knowledge of multi-scale flow instabilities. The characteristics of pulsed flow, despite complexity, are promising for increasing system efficiency by reducing mass flux while simultaneously reducing undesirable boundary layer vortices.

The success of pulsed flow actuators depend mainly on their pulsing frequency range, momentum addition into the environment, and overall system size versus complexity. Broad bandwidth potentially allows for a reduction in power and a greater level of adaptability to various applications and flows. It has been shown that high momentum input with supersonic microjets proves to be more effective than low momentum addition, especially when ambient flow velocities are high [9, 10]. Microjets are adept with high momentum addition due to their small diameter when coupled with large momentum flux [14].

The robustness of micro-actuator designs rely on advances in the actuator dynamics over a broad range of ambient conditions accompanied with a high cyclic lifespan. Piezoelectric materials are an ideal candidate to aid in achieving these performance attributes. When an electric field is applied to a piezoelectric material, mechanical strain is generated and conversely, stress induces a charge [15]. The actuator characteristics of piezoceramics include high forces and large bandwidth in a compact actuator. However, strain of these ceramic stacks is on the order of about 0.1 %. Addressing the issue of increasing actuator displacement while maintaining a small size and high displacement is important for active flow control of aerospace structures.

The concept of utilizing smart materials such as piezoelectric actuators for flow control has been considered in a number of adaptive structure designs. Piezoelectric based diaphragms, flaps, cantilevered beams, etc. have been used for low momentum control of cavity flows and boundary layer shear flows [7, 16, 17]. However, combining the closed-loop tunability of a piezohydraulic stack actuator with the concepts of steady mass flow microjets presents new design capabilities [9, 18, 19]. An actuator is developed and tested here that integrates these two subsystems together to produce active broadband pulsed microjet flow. The design integrates a 400 μm diameter microjet with a piezoceramic stack coupled with a hydraulic circuit to create a high speed pulsed flow control valve.

The stack actuator's 20 μm maximum displacement is amplified using a hydraulic circuit to deform a rubber diaphragm. This diaphragm throttles the flow through the 400 μm diameter microjet. The design characteristics, system dynamic modeling, experimental set-up, and experimental results including micro-Schlieren flow imagery and exiting flow dynamic pressure measurements of the actuator are presented.

2   Actuator Design and Modeling

The design of the piezohydraulic actuator design is given followed by the experimental set-up. Within the description of the actuator design, a nonlinear system dynamic model is described and compared to quasi-static actuator performance. Predictions of broadband actuation are also given. The modeling was used to understand the dynamic performance and limitations of the actuator to facilitate microjet flow control experiments.

2.1   Piezohydraulic Actuator Hardware Design

The piezohydraulic actuator is comprised of six main components; a piezoceramic stack actuator, piston, two rubber diaphragms enclosing hydraulic fluid, a cylindrical aluminum housing, and a microjet. The piezoceramic stack actuator (Kinetic Ceramics) that is positioned inside the aluminum housing is cylindrical in shape with a length of 22 mm and a diameter of 19 mm. A nominal free stack actuator displacement of $\sim$20 μm is achieved at 1 kV. Under fixed displacement boundary conditions, the stack is expected to generate 10 kN based on published data (Kinetic Ceramics). A dual-diaphragm design, using a large rubber gasket next to the piston and a small rubber gasket at the top of the converging nozzle, encloses silicone hydraulic fluid (Dow Corning 200) with a viscosity of 0.65 cSt. The design of this actuator is illustrated in Figure 1.

Hydraulic amplification is utilized to substantially increase displacement relative to the piezoceramic stack actuator. The amplification is achieved using a converging nozzle design, shown in the top portion of Figure 1. By applying an electric field to the stack actuator, strain is applied to the piston which forces the hydraulic fluid into the cylindrical channel to deform the smaller rubber diaphragm. Fluid is forced through the chamber above the piston into the smaller cylindrical channel. The amount of deformation in the stack actuator and top rubber diaphragm is dependent upon the bias pressure applied to the hydraulic fluid, the voltage supplied to the piezoelectric stack actuator, and the initial piston location relative to the initial location of the smaller rubber diaphragm. Hydraulic amplification of $\sim$65 times has been achieved between the stack actuator and the smaller rubber diaphragm located at the top of the actuator housing [20].

2.2   Microjet Interface

By coupling a 400 μm diameter microjet with the deforming rubber diaphragm, an active broadband pulsed microjet is created. The smaller rubber diaphragm, used to seal the hydraulic fluid at the top of the converging channel, is fixed between the actuator housing and a microjet made of acrylic. The rubber diaphragm deforms into the flow path whenever voltage is applied to the piezoeletric stack actuator causing an obstruction to the flow. Whenever a sinusoidal input voltage is supplied, the microjet flow varies as a sinusoidal pressure or flow. Figure 2 illustrates the microjet interface including the junction between the hydraulic actuator housing and the acrylic microjet as well as the interaction between the rubber diaphragm and microjet airflow.

Testing of actuator intially focused on quasi-static performance characterization and a system dynamic model to validate electro-fluid-mechanical dynamic performance [20]. These experiments
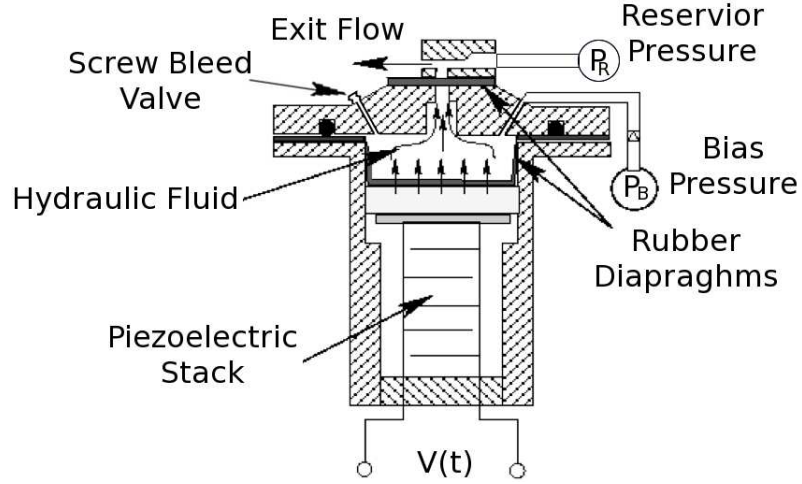
Figure 1: Cross section view of the piezohydraulic actuator.

consisted of a modified microjet interface structure that allowed a capacitor probe access to the top diaphragm displacement. During these experiments, significantly large, bi-stable displacements were quantified. Through model predictions the deformation was found to be predominantly due to snap-through buckling instability of the top diaphragm. Due to this nonlinearity, estimates on the frequency response were calculated based on a simple linear analysis. The results suggested that a bandwidth of 1 kHz was achievable. Direct measurement of high frequency diaphragm behavior was not trivial; therefore, the system was modified to conduct pulsed pressure and flow experiments.
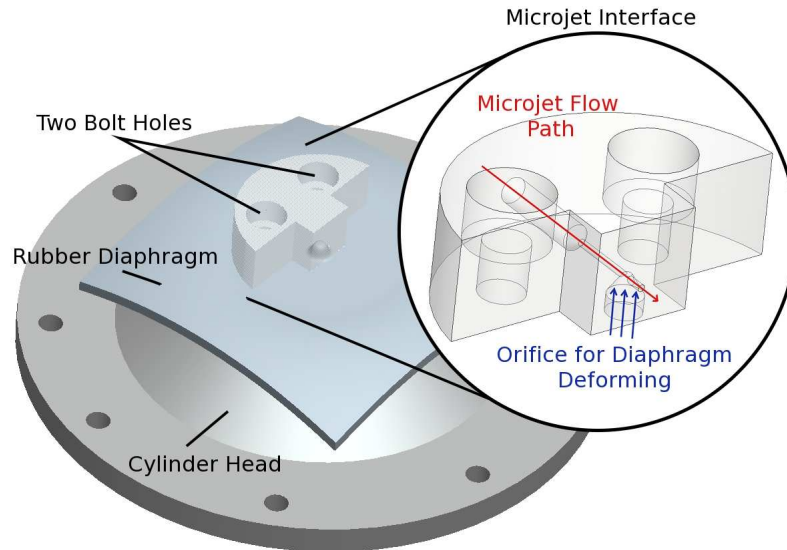

Figure 2: Rendering of microjet interface with diaphragm and cylinder head.

2.3   Multi-physics System Dynamic Modeling

The basic governing equations summarizing the system dynamic model are given here. More details can be found in [20]. The purpose of developing this model was to ensure a sufficient understanding of the internal, nonlinear dynamics associated with the observed displacement amplification. In addition, predictions of broadband actuation were made to estimate key limits associated with high frequency pulsed actuation prior to conducting pulsed flow pressure and flow visualization measurements.

The system dynamic model compares linear piezoelectric and nonlinear ferroelectric constitutive behavior of the stack actuator, viscous hydraulic fluid flow within the cylinder head, and hyperelastic stress-strain behavior of the top diaphragm that is coupled to the hydraulic pressure and is used to throttle the microjet. The nonlinear ferroelectric model is based on a physics-based homogenized energy framework that couples Boltzmann's relations with rate-dependent polarization evolution and mechanics coupling [21]. In compact notation, the model is described by

$$\dot{\mathbf{x}}(t) = \mathbf{A}(\mathbf{x})\mathbf{x}(t) + [\mathbf{B}(u)](t)$$
$$y(t) = \mathbf{C}\mathbf{x}(t)$$

(2.1)

and subjected to a set of initial conditions $\mathbf{x}(t = 0) = \mathbf{x}_0$. The state vector, $\mathbf{x}$, includes the displacements and velocities of the stack actuator and rubber diaphragm and pressures within the cylinder head. The matrix, $\mathbf{A}(\mathbf{x})$, is a function of the rubber diaphragm displacement due to the form of the hyperelastic constitutive equation used to describe its deformation. The input operator, $[\mathbf{B}(u)](t)$, is written as a nonlinear function when nonlinear ferroelectric behavior is included in the model. The scalar input u is the electric field applied to the stack actuator. For brevity, the details of these governing equations are omitted but can be found in detail in [20].

Due to the nonlinearity of the differential equations, the system of equations is solved numerically using a temporal discretization at time steps denoted by $i = 1, \ldots, N$ and time step Δt. The solution of the state equations at the end of each time step is used as the initial condition for the next iteration. Using the central difference method, the discrete form of (2.1) is

$$\mathbf{x}_{i+1} = \left(\mathbf{I} - \frac{\Delta t}{2}\mathbf{A}_{i+1}\right)^{-1}\left[\left(\mathbf{I} + \frac{\Delta t}{2}\mathbf{A}_i\right)\mathbf{x}_i + \Delta t\mathbf{B}(u)\right]$$

(2.2)

where the subscripts denote each time step defined over the time interval $[t_0, t_f]$ with uniform mesh having a size Δt at points $t_0, t_1, \ldots, t_N$.

The computational results and comparisons with experiments are illustrated in Figure 3 and 4. After fitting the ferroelectric model to data at multiple frequencies (Figure 3), the results were applied to the fully coupled piezohydraulic system dynamic model. The results of the top diaphragm displacement, as illustrated in Figure 5, shows good model prediction when minor loop hysteresis from ferroelectric behavior is included in the model. Despite these losses, good bandwidth is predicted up to 1 kHz based on model estimates. It will be shown in the experimental section that these model estimates reasonable predict pulsed microjet flow when the diaphragm is used to control gas flowing through the top microjet interface.

After modeling and characterizing the quasi-static behavior, preliminary test were conducted to understand the dynamic flow and pressure response at the microjet nozzle exit [22]. The preliminary data illustrated pulsed flow up to approximately 600 Hz before attenuation occured. Later, a set of rigorous pressure and flow visualization tests were conducted using micro-Schlieren photography and displacement strain data to illustrate the various phases of the pulsed flow at frequencies ranging between 1 Hz to 1.6 kHz. This data will be presented after describing the experimental set-up.
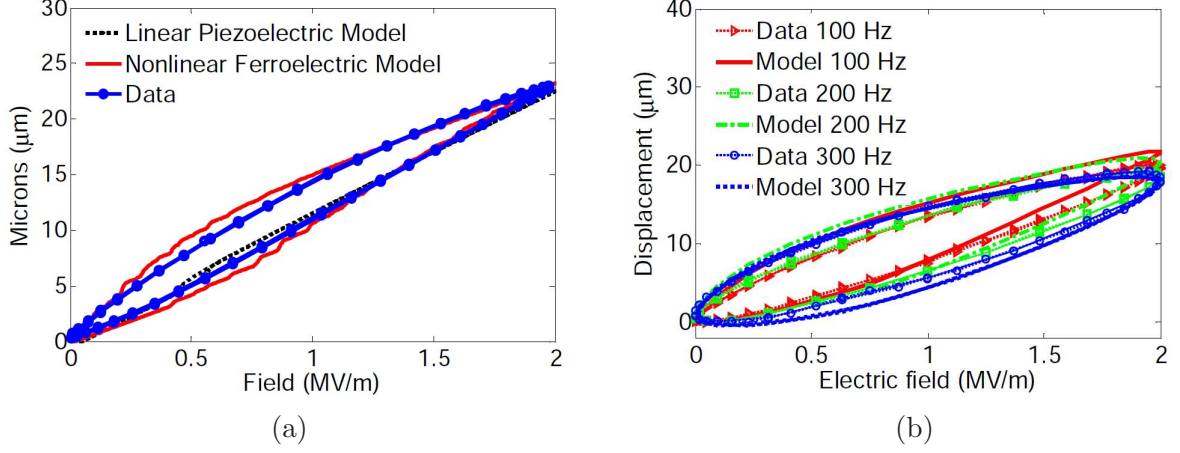
Figure 3: A comparison of the piezoelectric stack actuator electromechanical behavior. (a) Quasi-static model comparison to linear piezoelectric behavior and the nonlinear ferroelectric model. (b) Rate dependent ferroelectric model predictions in comparison with data.

3 Experimental Setup

In this section, two different experimental set-ups used to characterize the piezohydraulic actuator are described. These two set-ups focus on 1) quantitative pressure measurements from a 400 μm microjet and 2) flow visualization during high frequency pulsed flow actuation. In comparison with
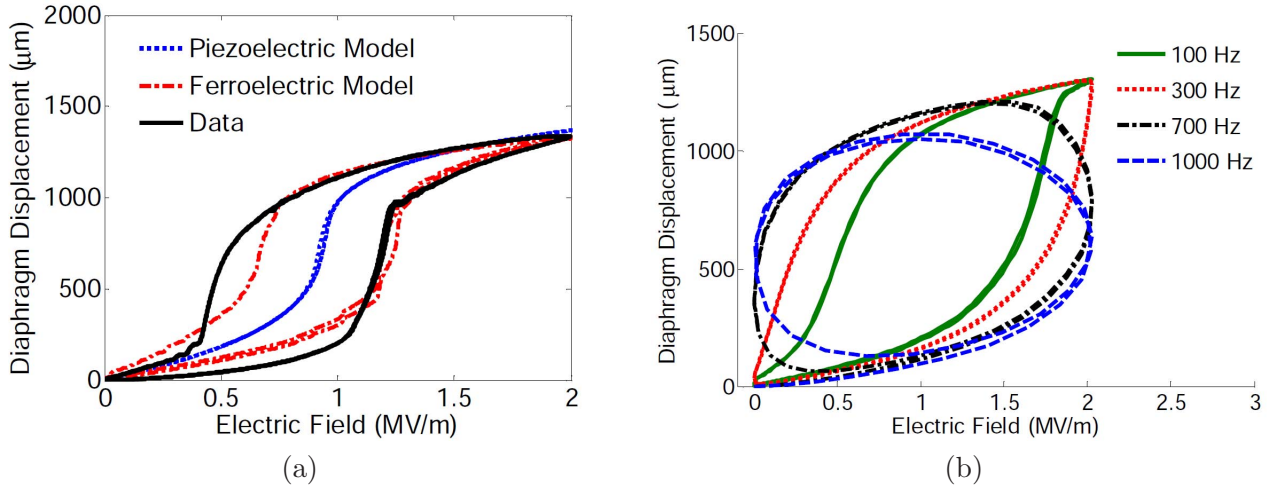

Figure 4: Model predictions of the displacement of the top diaphragm in Figure 5. A modified microjet interface and non-contact capacitor probe were used to conduct the measurements, see [20]. (a) Comparisons of the ferroelectric and piezoelectric stack actuator models with data. (b) Estimates on high frequency displacement actuation up to 1 kHz.
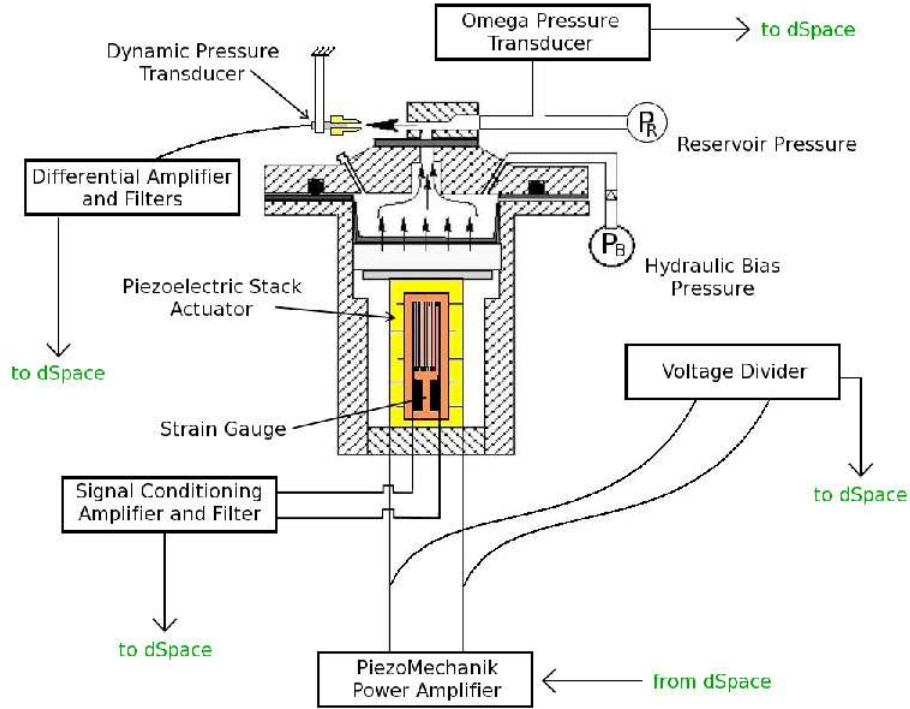
Figure 5: Schematic of testing components and signal routing in relationship to the piezohydraulic actuator.

Figure 1, several experimental measurement components used in characterizing the piezohydraulic actuator are shown in Figure 5.

The assembly of the hydraulic actuator system consists of a hydraulic circuit and the hydraulic actuator illustrated in Figure 6. The hydraulic circuit acts as a means to charge the hydraulic actuator with silicone fluid, purge air from the system, and control the bias pressure and the preload that is simultaneously applied to the rubber diaphragm and piezoelectric stack actuator. A nitrogen tank is used as the bias pressure source of the hydraulic circuit. An accumulator is used to apply a constant bias pressure to the piezohydraulic actuator during testing. A digital pressure gauge was placed in-line after the accumulator to monitor bias pressure during testing. A check valve is used to prevent hydraulic fluid from flowing back into the accumulator. A shut-off valve is connected after the check valve to allow for pressure to be bled off from the hydraulic actuator without affecting the pressure maintained in the accumulator. Air is bled from the system via a bleed valve within the cylinder head. To bleed air from the system, the accumulator is charged with pressure while the shut-off valve is open and the screw valve is slowing unscrewed. This relieves pressure from the system and allows air to be evacuated. Any entrained air inside the hydraulic circuit between the check valve and the hydraulic actuator can significantly reduce the amount of hydraulic amplification.

The following equipment was for testing and data collection. The piezoelectric stack actuator is powered by a PiezoMechanik 1000V/7A switching power supply to amplify the input voltage signal. The input signal was generated using a dSpace data acquisition system (DS1005 DSP board), controlled by Matlab and Simulink. The input signal to the PiezoMechanik amplifier ranged from 0
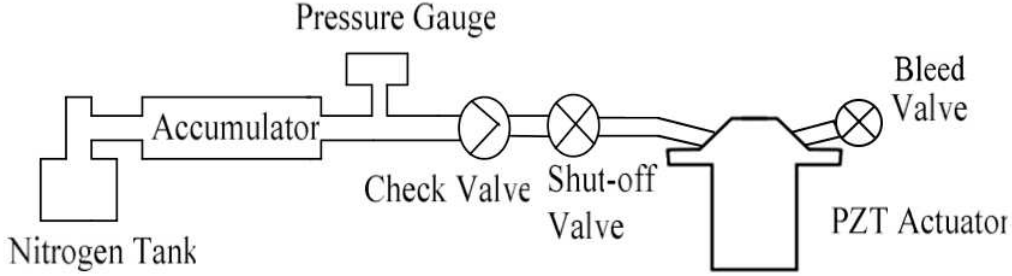
Figure 6: Schematic of the hydraulic system used to charge the piezohydraulic actuator with fluid and remove entrained air.

to 5 volts. The amplifier increased the voltage by a gain of 200 to achieve a signal ranging from 0 to 1000 V. The amplified signal was monitored with a voltage divider to quantify output voltage applied directly to the stack actuator. During operation, dSpace was used to collect data for the displacement of the stack actuator via an Omega strain gauge, an SGD-10/350-LY11, and the unsteady pressure measurements of the exiting flow from the microjet interface using a Kulite pressure transducer. The dynamic response of the strain gauge was initially characterized using a Lion Precision C1-A capacitor probe to measure displacement for the test range of input frequncies. The dSpace system was also used to monitor the reservoir pressure using an Omega PX215-100AI pressure transducer for the supplied flow into the microjet. A Vishay 2310B signal conditioning amplifier was used for filtering and amplifying the signal from the Omega strain gauge. A 0-100 PSIG range Kulite pressure transducer, model number XCQ-062-100G, with a sensitivity of 1.002 mV/PSIG was supplied power and signal amplification using a Hendrick and Assoc. Mx9000 differential amplifier and filter.

The dynamic pressure transducer created an issue for direct implementation within the test setup. In preliminary tests, a similar Kulite dynamic pressure transducer was used to collect normalized unsteady pressure data. The setup for this probe is shown in Figure 7. In this test configuration, the data collected by the probe could not be scaled to determine pressure due to the probe's size and would lead to uncertainty in the pressure measurement. Both dynamic probes have an outer diameter of 1.6 mm; four times the size of the microjet exit. The screen, depicted in Figure 8(a), mounted to the probe also created the issue of pressure being applied unevenly to the inner pressure diaphragm. To precisely calibrate the unsteady pressure collected, a brass nozzle was attached to the end of the probe. The brass nozzle has an inner diameter equal to that of the microjet to reduce measurement uncertainty. It was attached securely using a rubber cement adhesive. The brass nozzle configuration is shown in Figure 8(b) and shown in the test apparatus in Figure 9. Once the nozzle was attached to the probe, the voltage signal into the data acquisition could be precisely scaled using the dynamic probe's sensitivity.

A micro-Schlieren optical setup was used to obtain flow visualization data from the exit of the microjet. This type of optical system was used to quantify the length scales associated with the exiting supersonic flow field. With a microjet diameter of 400 μm, a spatial resolution on the order of tens of microns is required. The micro-Schlieren setup includes a high-magnification in-line achromatic lens based optics coupled with a knife edge and a Kodak Megaplus™ 1.4 camera with a resolution of 1008 by 1018 pixels. A knife edge was selected for the setup compared to a gradient
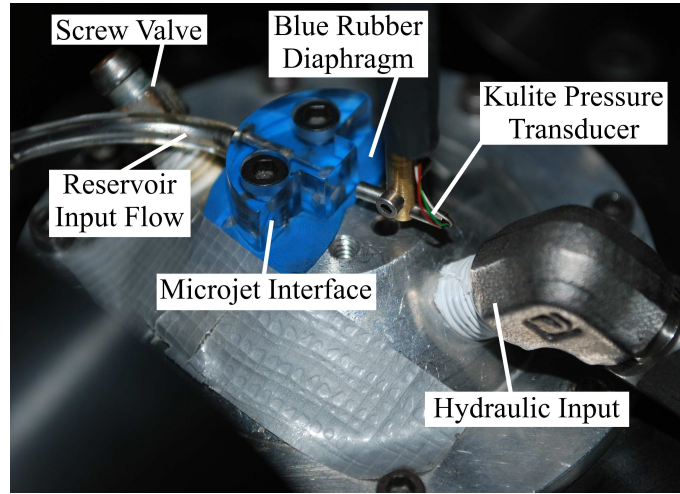
Figure 7: Close up view of the Kulite pressure transducer and microjet interface.

filter for better sensitivity. An IDT LED connected in-line with a Stanford model DG535 delay/pulse generator provided a strobing light source. The final magnification of the optical setup was in the range of 4-5x. The micro-Schlieren setup with the hydraulic actuator system positioned for testing is shown in Figure 10. It should be noted that the pressure probe in Figure 7 was removed during these measurements to avoid impinging flow fields during pulsed flow actuation.
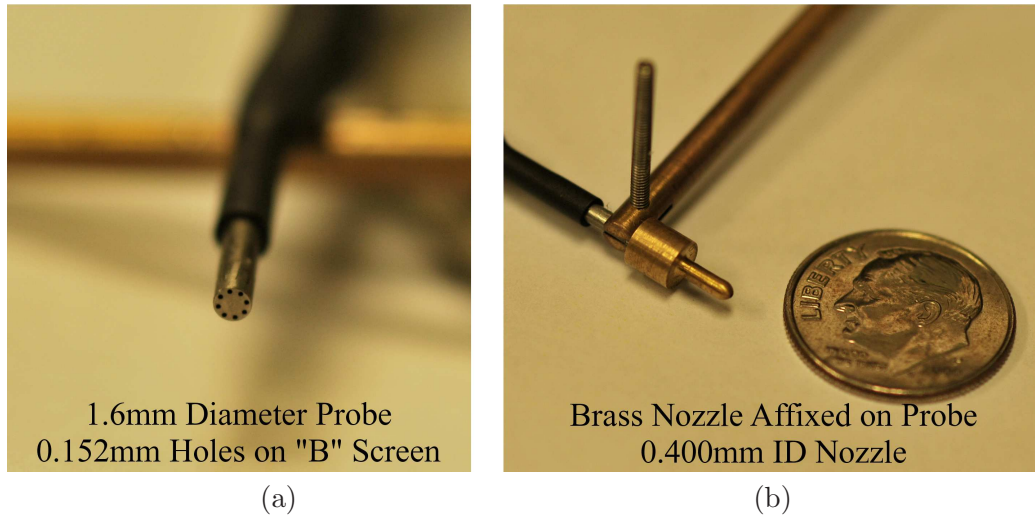

Figure 8: (a) Close up view of unaltered dynamic pressure probe. (b) Close up view of brass nozzle attached to probe with a quarter for size comparison.
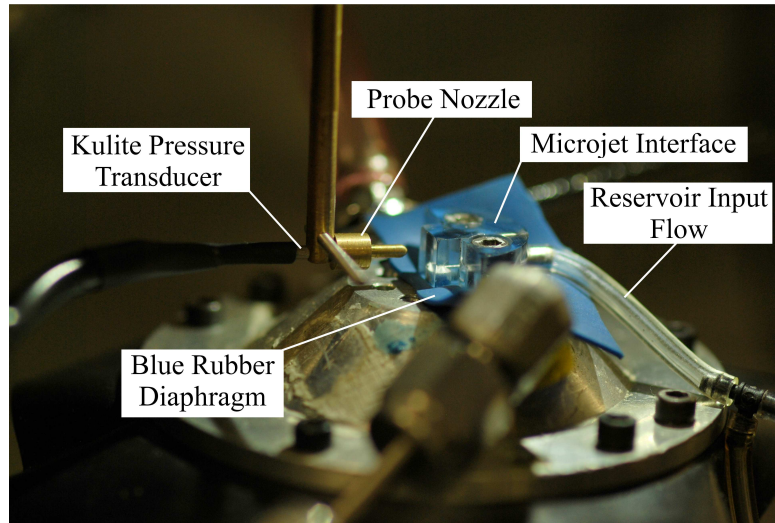
Figure 9: Close up view of the Kulite pressure transducer with affixed brass nozzle configuration in test apparatus.

3.1 Experimental Methods

Experiments were conducted at the Advanced Aero Propulsion Laboratory (AAPL) at Florida State University. Bench-top tests were arranged on an optical table to facilitate micro-positioning and to mitigate environment vibrations. Flow characterization measurements were taken at 1 Hz as a baseline input frequency and at 100 Hz increments up to 1.6 kHz input frequencies to the
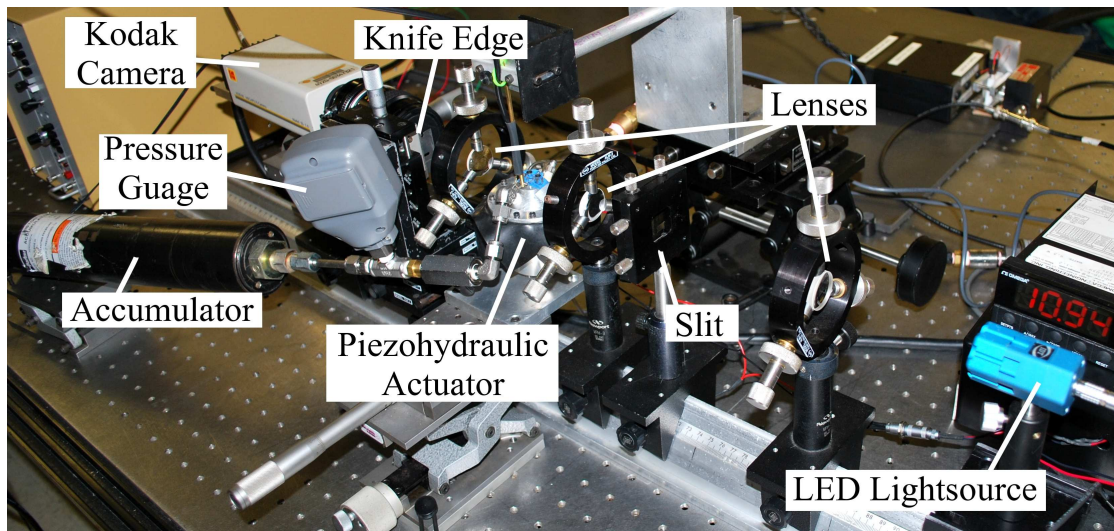

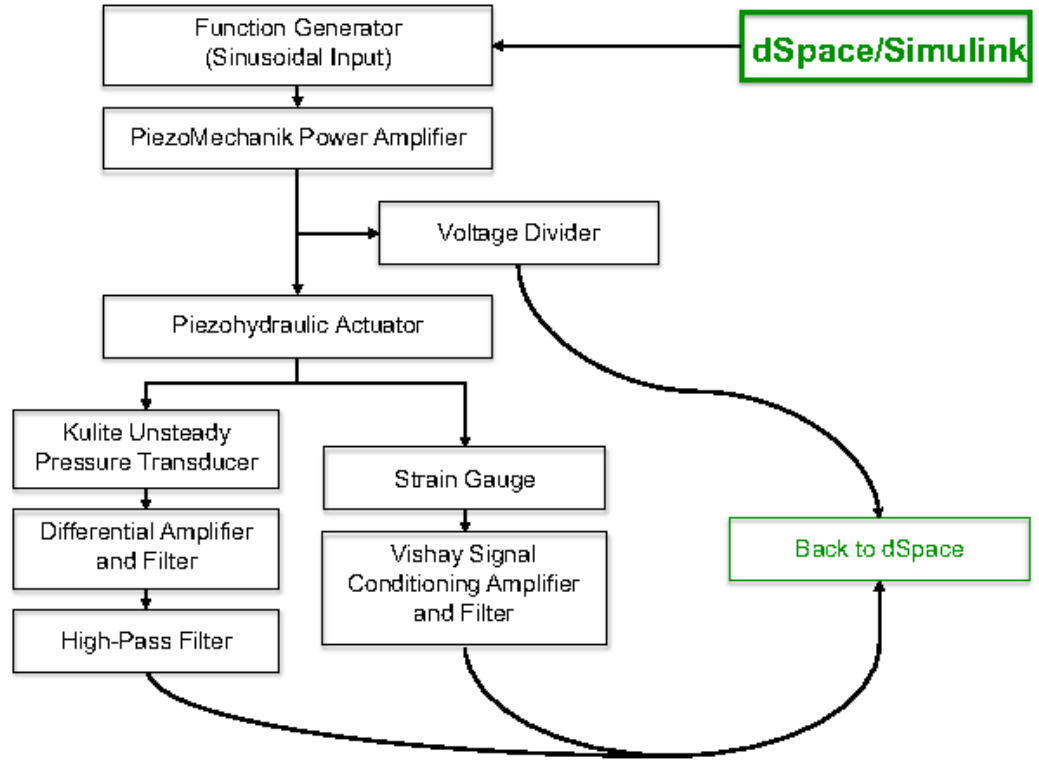Figure 10: Micro-Schlieren optical setup.

Figure 11: Block diagram of the signal routing and data acquisition during pulsed flow pressure response testing.

piezoelectric stack actuator. Parameters such as the reservoir pressure supplied to the microjet and the output signal high-pass filtering were kept constant throughout test series. Test specifics are provided for each set of data. The bias pressure supplied to the accumulator ranged from 45-55 psig. This range was selected to optimize the microjet performance. For example, larger bias pressure was required for an increase in microjet air pressure to sufficiently throttle the microjet flow.

Data collected with dSpace included the exit flow dynamic unsteady pressure, input reservoir pressure for the microjet, and the piezoelectric stack strain. This data was collected simultaneously with the input voltage and amplified voltage signal that was applied to the stack actuator. When collecting micro-Schlieren images, dSpace was also used to provide a control step input for the camera frequency and LED light source. IDT's proVision™ software was used on a separate computer to collect images from the Kodak Megaplus™ camera. A schematic of the drive electronics and signal routing is shown in Figure 11 for the pulsed flow pressure response characterization, and in Figure 12 for micro-Schlieren flow imagery.

The piezoelectric stack actuator was driven using a switching power amplifier that requires adjusting the input voltage range to avoid certain nonlinearities due to saturation in the output signal below 60 V. Before tests with the piezoelectric stack were conducted, the strain gauge amplifier was balanced without any electrical load to the stack. This was defined as the zero reference strain prior
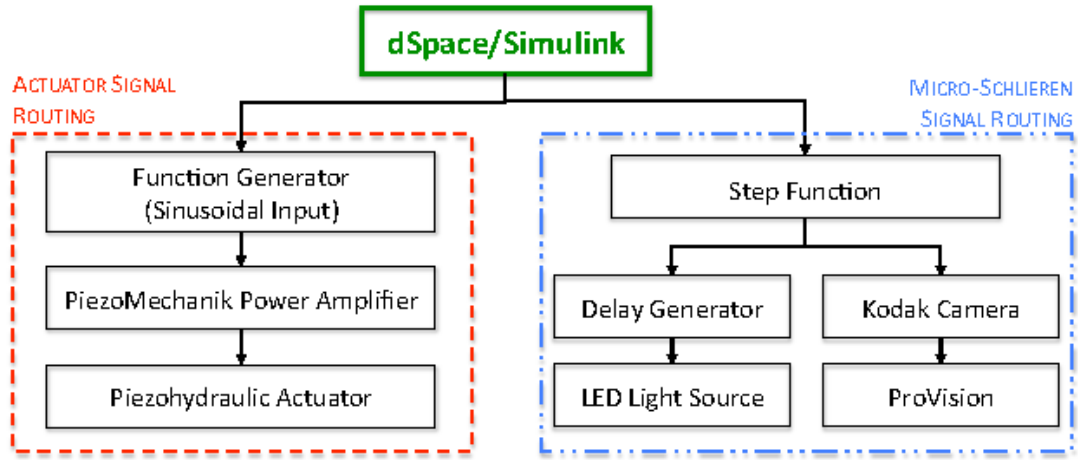
Figure 12: Block diagram of the signal routing and data acquisition for micro-Schlieren flow imagery testing.

to applying the small bias voltage from the switching power amplifier. The power supply has a bias voltage of approximately 60 V which is evident during experiments since the displacement during low frequency tests never approaches the reference zero displacement when the strain gauge amplifier was balanced with the power amplifier off. The sinusoidal input signal to the stack was also biased to approximately 80 V to reduce the possibility of saturation at the lower peak of the sine wave. This is especially important at higher frequencies to reduce stack damage and actuator nonlinearities from a saturated voltage signal. The voltage applied from the power amplifier to the piezoelectric stack actuator was also monitored using a voltage divider that reduces the voltage signal by 200 times.

Performance of the piezohydraulic actuator was conducted using two procedures. For exit flow imagery, the micro-Schlieren system was used for tuning the actuator for performance during image capture while adjusting the bias pressure to the accumulator to optimize the throttling effect of the rubber diaphragm and microjet interface. The shock shell sizes coupled with the input pressure and microjet geometry were used to calculate and check the exit flow speed [23]. Compared to tests utilizing the dynamic pressure probe, the micro-Schlieren testing required this method of tuning to maintain and maximize performance. No pressure data was collected during image capturing. For exiting flow pressure characterization, the dynamic probe was used along with micro-positioning stages to fix the probe's position at certain distances away from the jet exit. Steady flow characteristics were found at the given input reservoir pressure with a 200μm diameter pitot probe at incremented distances away from the microjet exit using steady flow to the microjet. This data was collected prior to pulsed testing to compare with the maximum output pressure of the throttled microjet at various pressure for the selected 0.25 mm position of the dynamic pressure probe which gave 25 psi static pressure.

Images of the flow were collected at a frequency of 25 Hz. This sampling frequency was used to collect multiple images of the flow at the same point in the high frequency actuation cycles. To obtain a complete series of images along a cycle of actuation, a delay was added between the applied voltage driving frequency of the stack actuator and the light-source and camera frequency in the Simulink software. A set of 25 images were collected for 25 different delays for each actuation frequencies.

Images at each delay were averaged to provide time-resolved steady-state pulsed flow visualization.

4 Experimental results

The piezohydraulic actuator was tested at frequencies ranging between quasi-static to 1.6 kHz to characterize pulsed flow behavior. These frequencies were chosen based on preliminary studies that demonstrated a drop in performance at ∼800 Hz and attenuated performance of flow over 1 kHz [22]. An input pressure of 30 psig was used for all dynamic pressure measurements. For micro-Schlieren testing, images were collected at 1 Hz, 400 Hz, 600 Hz, and 800 Hz. These frequencies were selected since they permitted the use of a constant phase collection of images at a 25 Hz sample frequency for micro-Schlieren testing. Two reservoir pressures of 30 psig and 40 psig were selected for the incoming flow to the microjet for image capture. Only images collected for the 40 psig tests are presented herein due to poor image quality at 30 psig. At steady flow operation of the microjet (i.e, no pulsing), the output flow was found to be supersonic as indicated by the formation of shock shells. New optical diagnostics have recently been developed in which additional tests are on-going to resolve finer flow features at different pulsed frequencies. *Preliminary results has demonstrated supersonic pulsed flow up to 1.2 kHz. The results will be summarized in a journal manuscript that will be submitted for review summer 2011.*

4.1 Pulsed Flow Characterization

Characterization of the piezoeletric stack was performed by measuring strain during pulsed flow tests. Two methodologies were used to characterize the strain: 1) *In situ* strain measurements were taken during all pulsed flow measurements using a strain gauge, 2) Capacitor probe (non-contact) displacement measurements were taken by clamping the piezoelectric stack between aluminum plates with plastic nylon bolts. The latter measurements were conducted to quantify uncertainty in strain gauge measurements. This was due to the fact that the strain gauges were applied to the exterior of the piezoelectric stack epoxy layer which can introduce uncertainty at higher frequencies if the epoxy exhibits viscoelasticity. This was found to be true as the frequency increased to approximately 400 Hz. Additional comparisons up to 1.6 kHz are given in [24].

The stack displacement, based on strain data, is shown in Figure 13. Strain gauge measurements were collected for frequencies up to 1.6 kHz. Additional verification measurements were taken with a capacitor probe aligned with the long axis of the stack. The capacitor probe was set for a high sensitivity with a peak to peak resolution of 6.18 nm and an RMS resolution of 1.32 nm. Comparison between the capacitor probe displacement measurements and strain gauge measurements are illustrated in Figures 14-16. As the input sinusoidal frequency for the piezoelectric stack increases, the uncertainty associated with the strain gauge increases. It is believed that viscoelastic effects may effect the strain gauge measurements since this gauge is mounted outside of the piezostack's epoxy layer. More data is needed, however, to confirm this behavior. The capacitor probe data is expected to be more accurate since this is a non-contact measuremet of a rigid plate that was firmly clamped to the stack actuator with nylon bolts. The actuator's blocked force is 10 kN; therefore, reductions in total strain were negligible as indicated by the quasi-static measurements. Further note that these measurements were not taken during hydraulic actuation.

Unsteady pressure was measured with the Kulite dynamic probe at a supplied reservoir pressure of 30 psig to the microjet. The probe was positioned 0.25 mm away from the microjet exit plane. At this distance, the open jet pressure was recorded with a 200 μm pitot probe to be ∼25 psig. This verified that the data collected with the dynamic probe at the same position also gave a steady 25 psig pressure. For each set of data collected, pulsed flow was first achieved at a baseline frequency
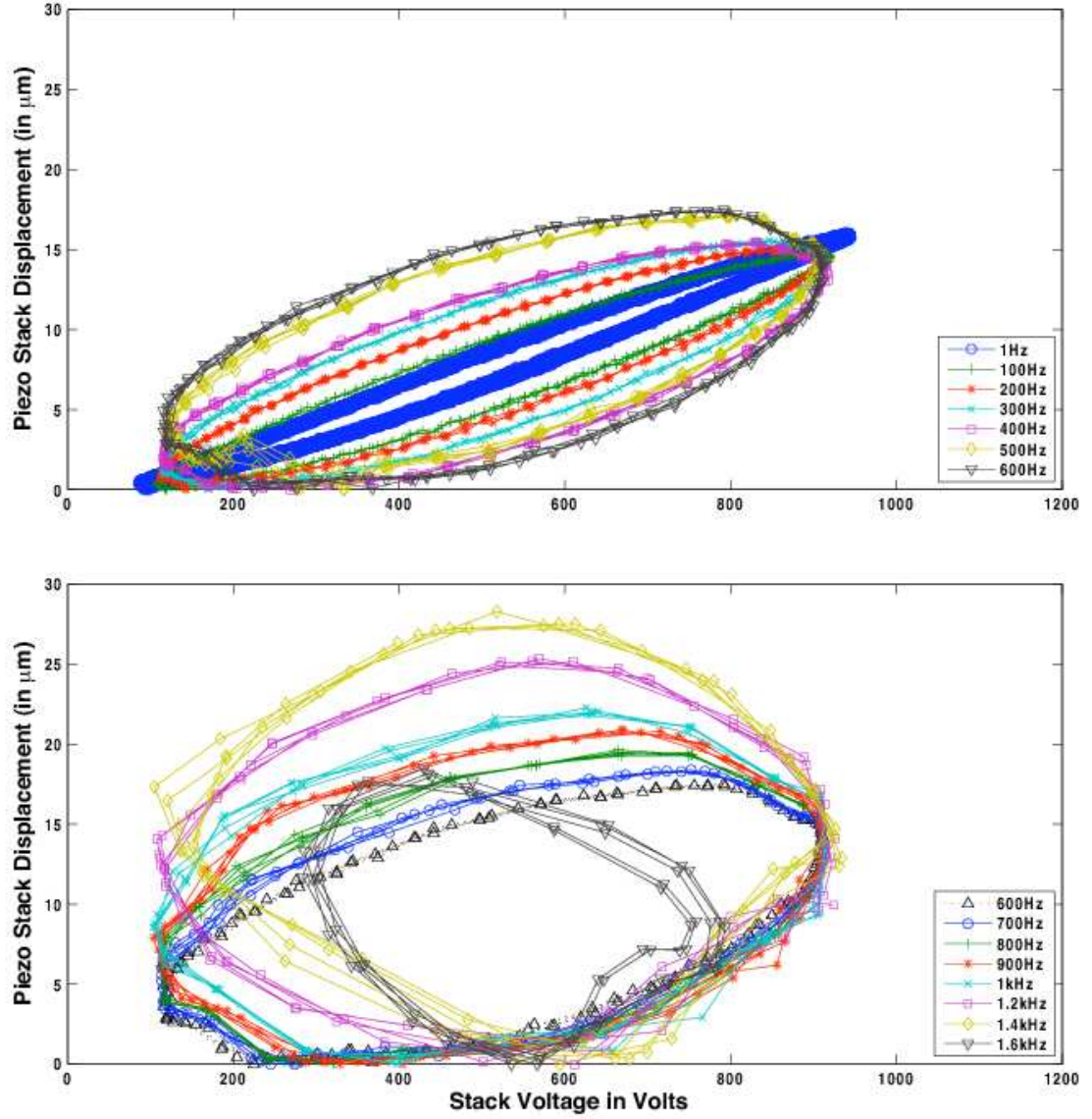
Figure 13: Piezo stack displacement versus applied voltage from power amplifier to piezoelectric stack during pulsed flow tests for each test frequency.

of 1 Hz with a maximum jet pressure approximately equal to the open flow pressure measurement. Data was then collected at each test input frequency, maintaining the same bias hydraulic pressure. However, for mid-range frequencies between 400 and 700 Hz, the bias pressure was increased from 45 psig to 51 psig to reduce "decoupling" between the rubber diaphragm and fluid flow. At these
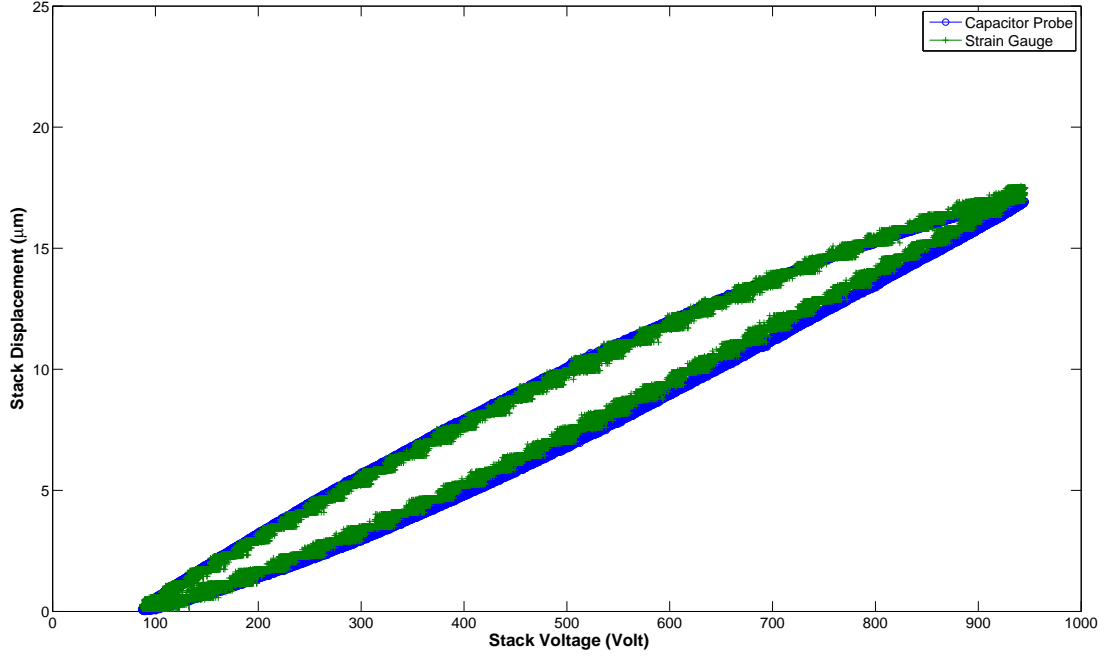
Figure 14: Displacement data for the piezoelectric stack actuator for an input frequency of 1 Hz.

frequencies the actuator would stop pulsing which is believed to be due to cancellations in the phases of the internal dynamics, although more analysis is needed to confirm.

A summary of the maximum, minimum, and peak to peak pressures for the microjet exit flow are given in Table 1. The peak to peak pressure response is plotted versus frequency in Figure 17. It is shown that there is little reduction in overall performance of the actuator for frequencies up to 400 Hz. For frequencies greater than 400 Hz, the performance slightly decays as the frequency increases. The overall performance of the actuator can also be established by examining the power spectral density of the pressure response from the microjet exit. Figure 18 shows the difference in the power spectral density between 100 and 1000 Hz. The power spectral density for other individual frequencies are illustrated in [24]. Attenuation around 10 dB is observed between the 100 Hz and 1.4 kHz tests.

4.2   Micro-Schlieren Flow Imagery

Figures 19-21 show micro-Schlieren images for various phases of the 400 μm jet pulsed at frequencies of 100 Hz, 400 Hz, and 800 Hz, respectively. Nine different phases of the microjet flow cycle are shown. As illustrated in Figure 19, the flow is supersonic for 100 Hz pulsed flow at certain parts of the cycle, while subsonic at other time increments, thus creating highly unsteady momentum. The supply pressure during these experiments was 40 psig in the micro-nozzle with a design Mach number of 1.0 at the nozzle exit. This is due to the nature of a converging nozzle which cannot have an exit Mach number higher than sonic velocity. The jet is underexpanded outside the nozzle which gives
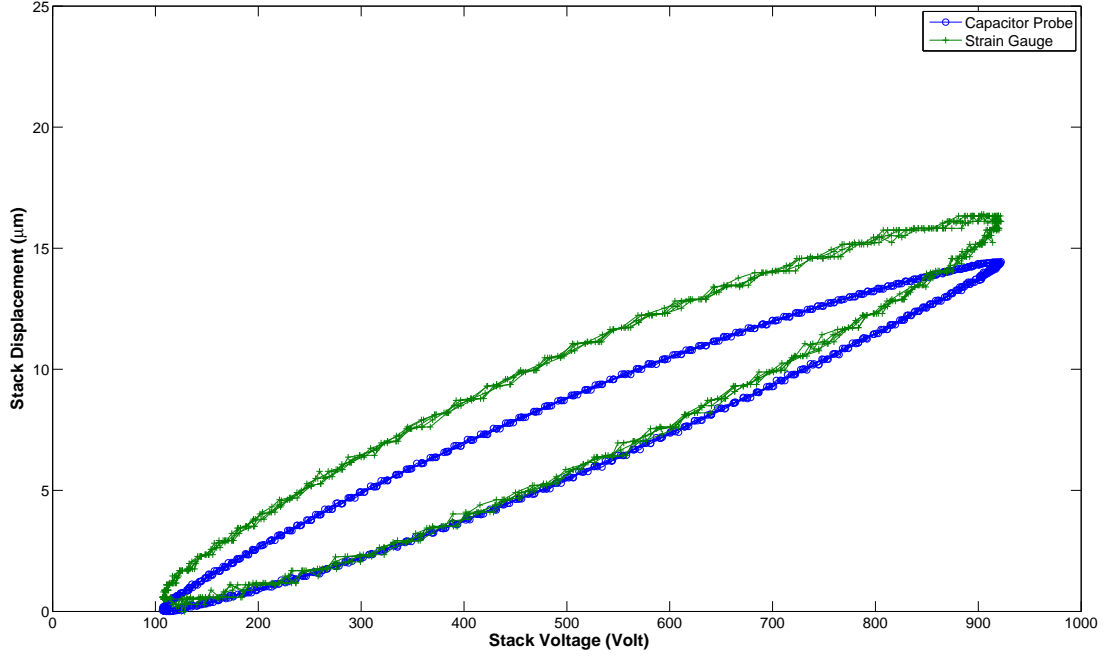
Figure 15: Displacement data for the piezoelectric stack actuator for an input frequency of 100 Hz.

an ideally expanded jet Mach number of 1.5. This Mach number calculation is an approximation for a source microjet pressure above 15 psig. The velocity of such an underexpanded jet is usually expressed as an ideally expanded jet velocity that can be calculated from the nozzle pressure to ambient pressure ratio. This ratio is approximately 3.8 which gives an ideal Mach number of 1.5 according to standard isentropic flow tables for compressible flow. The bounds on the true Mach number are between 1 and 1.5.

Pulsed flow at higher frequencies is also quantified with the micro-Schlieren images. At 400 Hz, the jet is also underexpanded which is evident from the presence of shock cells in the flow. This shows the capability of the actuator for generating unsteady supersonic jets at a higher pulsing frequency. Similar results are obtained at 800 Hz, as shown in Figure 21. The momentum has been reduced at this higher pulsing frequency as illustrated in Figure 21. The reduce shock cell strength in Figure 21 indicates that the higher pulsing rate causes a lower Mach number outside the nozzle; however, the flow is still supersonic at certain phases of the cycle.

5   Next Generation Actuators

The piezohydraulic pulsed microjet actuator has provided a broadband flow control device that can be used as a benchmark testing device to understand how to control flow such as dynamic stall on rotorcraft as well as noise emission reduction. However, one of the challenges with this design is the size and reliability associated with hydraulic fluid. This creates challenges in its practical use within thin rotorblades. Therefore, this project has included, in parallel, the development of a
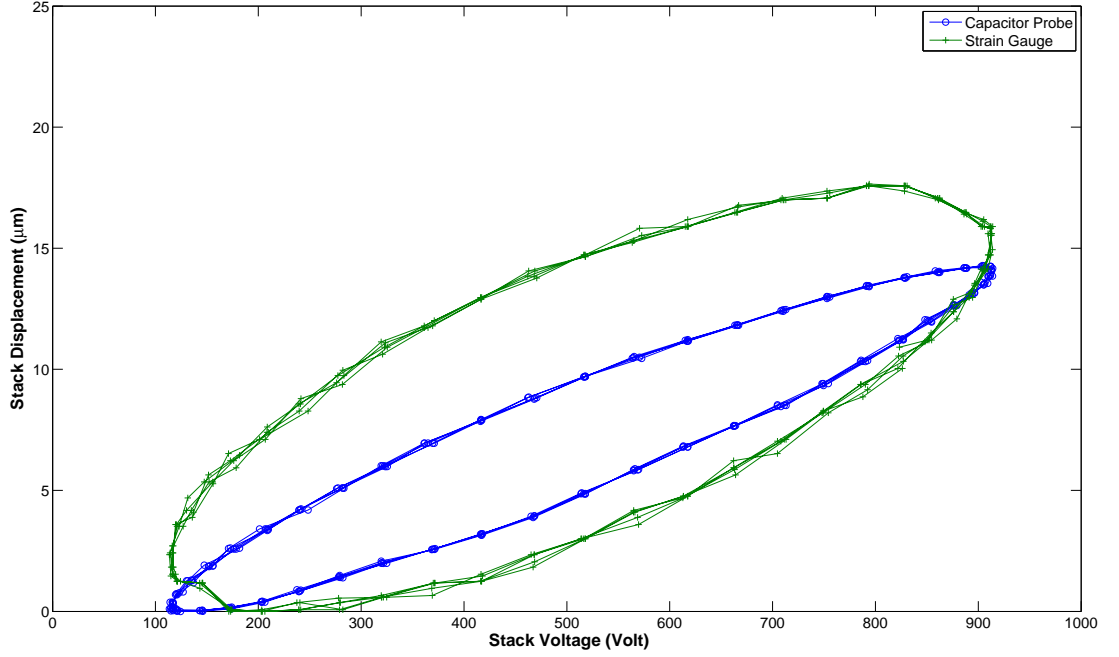
Figure 16: Displacement data for the piezoelectric stack actuator for an input frequency of 400 Hz.

broadband piezoelectric pulsed actuator that eliminates hydraulic fluid and takes advantage of an actively morphing supersonic nozzle to control the exit flow. It is described in the following section.

In addition, partial support through this ARO project has resulted in the development of a resonance enhanced microjet (REM). A brief description of the design, experimental results and high fidelity aero-acoustic simulations are presented. This microjet actuator utlizes a single microjet as a source that blows air into a small resonant cavity that contains microjets at the opposite end of the cavity. The cavity resonator results in pulsed actuation at the exit. This actuator is relevant to the active morphing project since it was demonstrated that large shifts in resonance can be achieved by changing the volume of the resonance cavity. Therefore, active structures could potentially be used to rapidly adjust the frequency for flow control and noise suppression applications.

5.1 A* Actuator

A converging diverging (CD) nozzle is commonly used to produce supersonic and steady flow at its exit. In our design, the CD nozzle design is coupled with a broadband piezoceramic stack actuator to create a novel, active supersonic microjet actuator which produces pulsed flow. By applying the precision and high frequency deformation of a piezoceramic stack actuator to the nozzle throat area (A*), at fixed exit area, a shape change occurs which results in a change in the exiting supersonic flow based on fundamental fluid dynamics.

The A* actuator system is devised of two main parts; the piezoelectric ceramic stack actuator and the converging diverging nozzle. The goal of combining these two components is to provide

19

Table 1: Pressure change of pulsed microjet flow with reservoir pressure of 30 psig at testing frequencies.

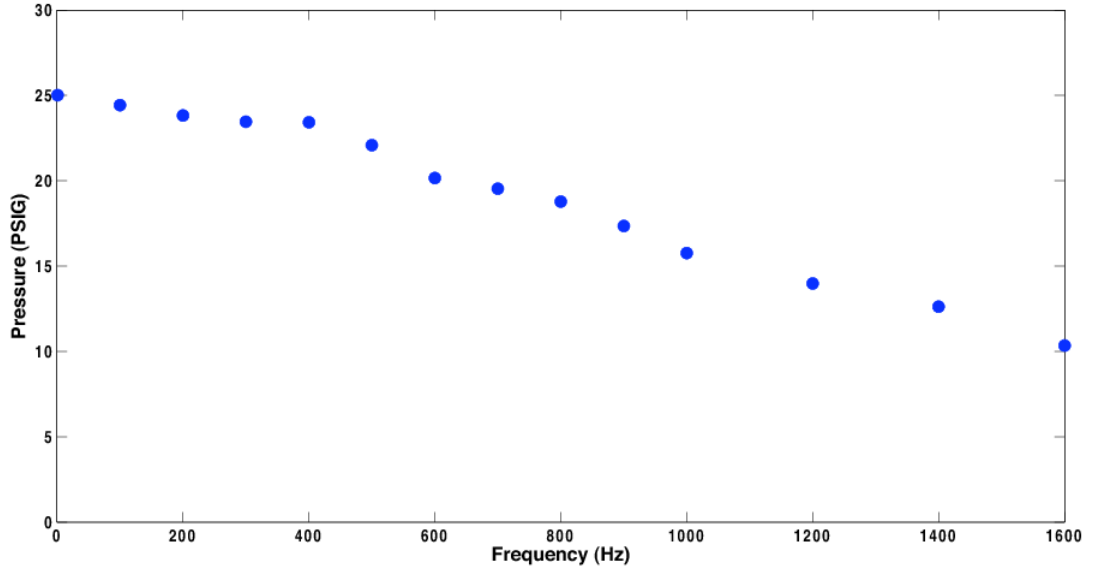| Frequency (Hz)	Maximum Pressure (psig)	Minimum Pressure (psig)	Peak to Peak (psig)
1	25.375	0.3662	25.0130
100	25.3448	0.9155	24.4293
200	24.7800	0.9613	23.8187
300	25.0397	1.5869	23.4528
400	24.9023	1.4801	23.4222
500	23.7579	1.6785	22.0794
600	24.0479	3.8910	20.1569
700	24.1699	4.6387	19.5312
800	22.4457	3.6700	18.7757
900	21.2402	3.8900	17.3502
1000	20.6299	4.8676	15.7623
1200	20.4468	6.4697	13.9781
1400	20.3094	7.6904	12.6190
1600	15.1062	4.7607	10.3455

Figure 17: Peak to peak exiting microjet unsteady pressure at an input reservoir pressure of 30 psig versus frequency range.

an adaptive supersonic microjet. The piezoelectric actuator allows for active control and tunable frequency over a broad bandwidth (1 Hz to ∼1 kHz). The CD nozzle allows for supersonic jet flow
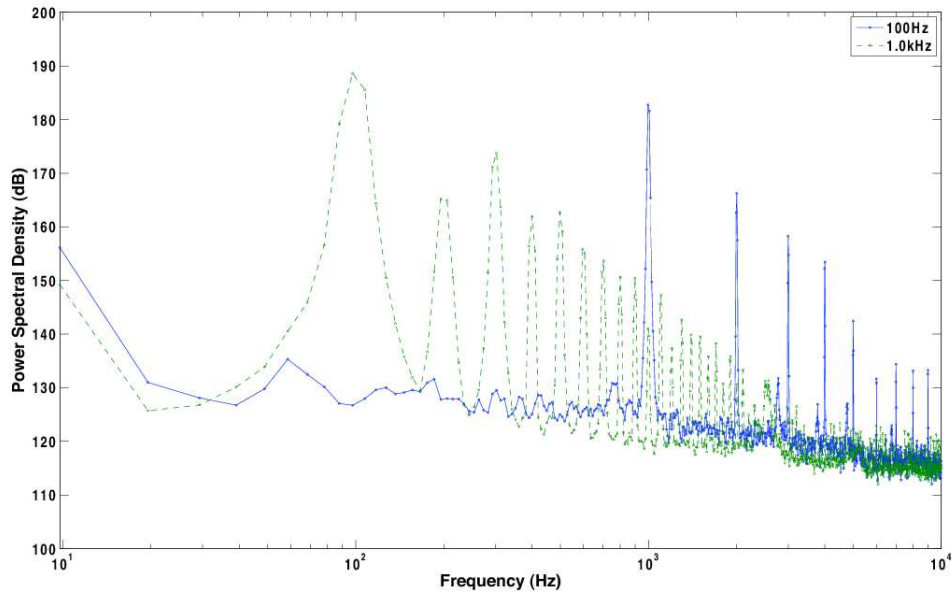
Figure 18: Power spectral density plot for 100 and 1000 Hz.

at the microjet orifice. A change in exiting jet flow occurs by actively controlling the throat area of the nozzle near the exit area. The CD nozzle is coupled to the actuator using a needle to precisely control the throat area as shown in Figures 22 and 23.

As shown in Figure 22, the first generation actuator is comprised of a piezoelectric ceramic stack actuator that is fixed at the base and an acrylic nozzle is located above the actuator which is also fixed to the base. A needle is attached to the top plate of the stack actuator to transmit force to the nozzle's throat. The initial actuator design has focused on ease of implementation and future designs will incorporate size and weight optimization for integration into aircraft structures. The design
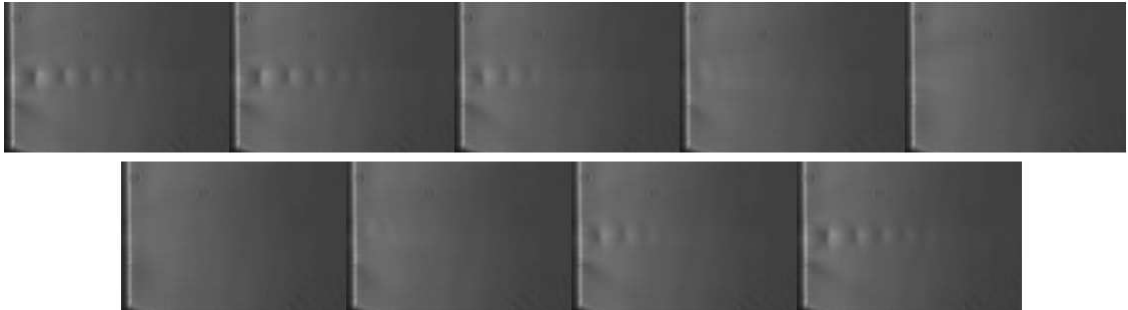

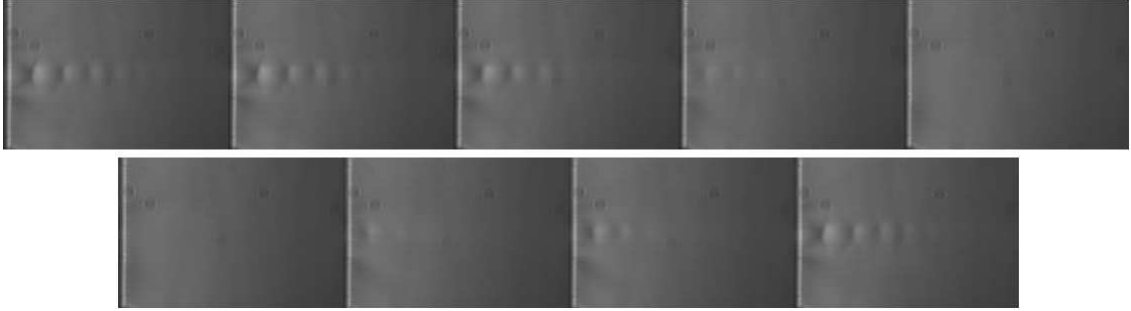Figure 19: Phase locked micro-Schieren images of pulsed jet at 100 Hz with a reservoir pressure of 40 psig.

Figure 20: Phase locked micro-Schieren images of pulsed jet at 400 Hz with a reservoir pressure of 40 psig.

utilizes four nylon screws to fix a plate to the top of the piezoelectric stack to ensure compression during operating to avoid microfracture and increase the piezoelectric response. Based on previous experiments, the nylon polymer deforms with the stack without any significant reduction in stack actuator deformation (18-19 μm). The needle mounted to the top plate is a type 304 stainless steel dispensing needle with an outer diameter of 304 microns.

The converging diverging nozzle was CNC machined out of cast acrylic. Acrylic was chosen due to its optical clarity for flow visualization and elastic behavior. COMSOL finite element modeling was used to determine if the acrylic deforms at the throat with a reasonable force without cracking or causing undesirable deformation at the nozzle exit; see [25] for details. The acrylic nozzle is machined in two mirrored halves. Due to the rectangular cross sectional area of the nozzle at the inlet, an adapter piece is also attached and sealed using a gasket to allow for incoming flow from any source.

The fabrication process for the nozzle begins with a stock piece of acrylic that must be machined into two mirrored halves. The outer dimensions are machined manually as well as the exterior mounting holes. Once the exterior shape has been finished, the nozzle face is placed facing up into a vice that holds it secure while the machine code for the nozzle and needle channels is executed on the HAAS Minimill. Once this process is complete for both sides of the nozzle, it is polished with
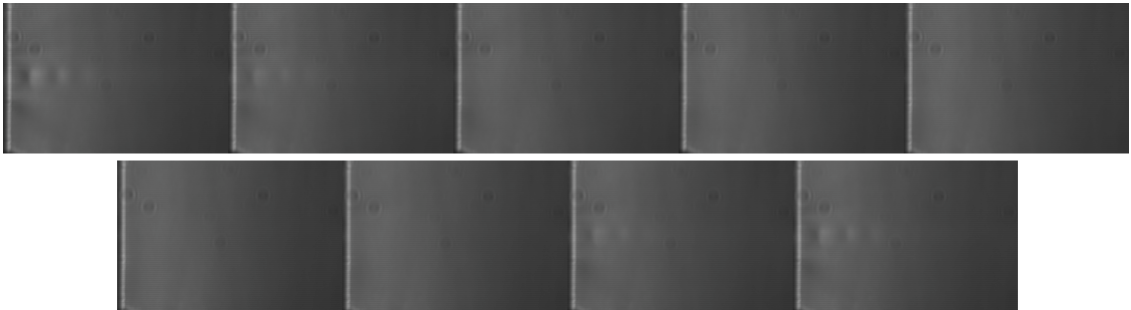

Figure 21: Phase locked micro-Schieren images of pulsed jet at 800 Hz with a reservoir pressure of 40 psig.
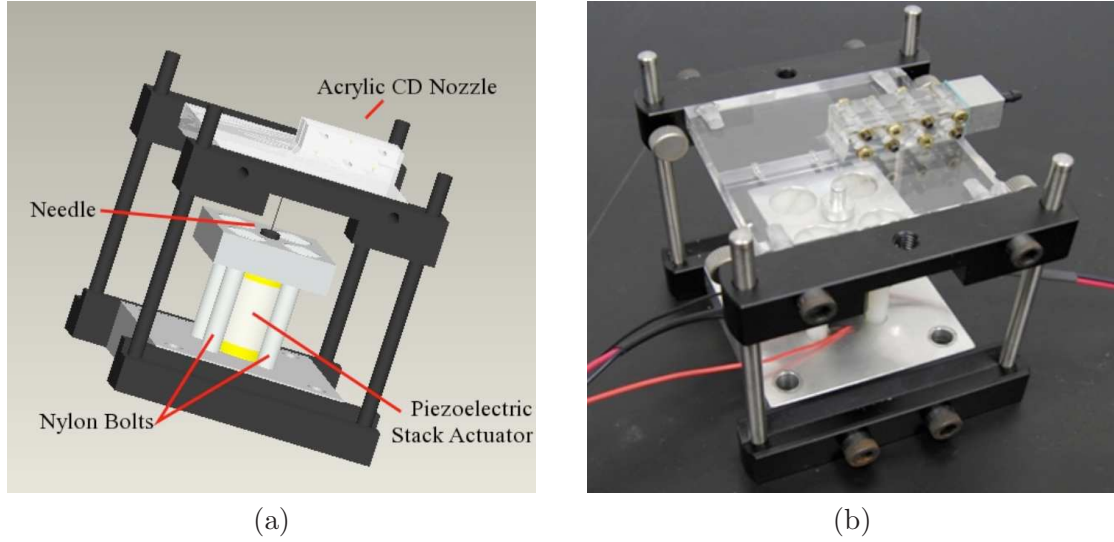
Figure 22: (a) Schematic rendering of the A* actuator. (b) Image of the first prototype.

up to 1200 grit wet sand paper and buffed until transparent.

An image of the CD nozzle is shown in Figure 23. The nozzle's dimensions were based on a magnitude of the change in throat area that closely optimized the change in momentum of the flow given our set of machining constraints. The nozzle was designed for an average exit Mach flow of 1.5. Using this Mach number and machining constraints, a corresponding throat width and height were chosen. The exit area dimensions were calculated by determining the critical throat area ratio based off the selected throat area. The incoming flow is allowed to become stable before entering the converging portion of the nozzle. The throat area of the nozzle is 300 μm high by 500 μm wide. The throat of the nozzle is uniform for a length of 300 microns to allow space for the needle and deformation of the acrylic. The nozzle's exit area is 350 μm high by 500μm wide. The width of the
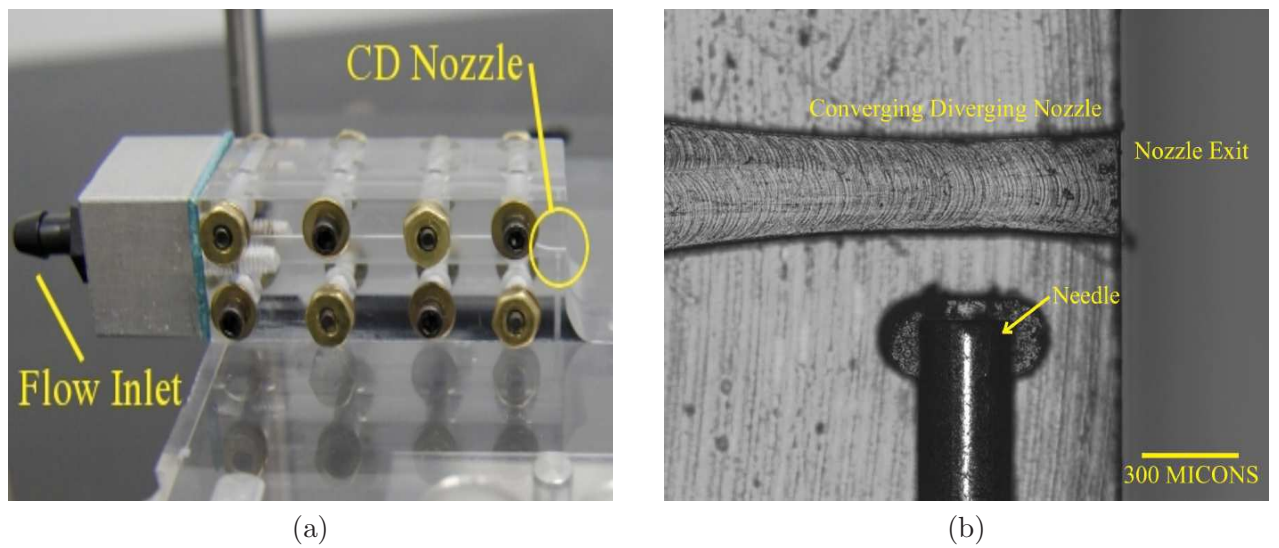

Figure 23: CD nozzle assembly and (b) microscopic view of the exit. The lower region is the location of the needle used to control the throat geometry via piezoelectric actuation.

nozzle is kept constant at 500 μm. A change in momentum of 9.60% is calculated with a change in flow from Mach 1.63 to Mach 1.34 as the throat of the nozzle deforms up and down. A channel is located 150 μm directly below the throat of the CD nozzle from the needle. The end of the channel has rounded corners to allow for adequate machine tooling space and reduce the stress concentrations that would result from sharp, rectangular corners.

The two acrylic halves of the nozzle are aligned via four dowel pins and secured together with eight bolts located above and below the nozzle. The acrylic nozzle assembly attaches to the stack actuator assembly using two optic rails. The rails provide horizontal adjustment of the acrylic nozzle for needle placement and allow the nozzle to be fixed during operation. The overall assembly was designed for the ease of testing and manipulation of the microactuator for future generation designs. The acrylic nozzle can easily be swapped or modified without any disassembly of the stack or testing equipment.

5.1.1 Experimental Implementation

The experiments were performed at the Advanced Aero Propulsion Laboratory (AAPL) of Florida State University. The same optical set-up used in the piezohydraulic actuator was used in these preliminary tests. Flow visualization tests were conducted in order to determine the flow characteristics and needle positioning of the first generation actuator. Air and carbon dioxide were used to visualize the output flow from the converging diverging nozzle. The piezoelectric stack actuator was not used during these preliminary tests. However, benchtop piezoelectric quasi-static deformation of the nozzle was checked under an optical microscrope. Minimal losses from the stack actuator displacement to the nozzle throat deformation were observed. The gauge pressure of the incoming flow was monitored using an Omega inline digital pressure transducer to assess if the supplied pressure was producing the desired supersonic flow. Due to the transparency of the acrylic nozzle, it is possible to position the needle precisely using the optical setup to determine when the needle comes into contact with the end of the needles channel.

The output flow of the converging diverging nozzle was tested for the design Mach number of 1.5. The incoming pressure was set at 53.95 psi (39.25 psi gauge pressure) to theoretically allow air to reach this supersonic speed. The resulting flow was found to be supersonic and underexpanded. Both carbon dioxide and air were tested at this pressure. Images from the micro-schlieren flow visualization under steady flow conditions are shown in Figure 24.

In summary, this actuator has been designed for supersonic flow in a region highly sensitive

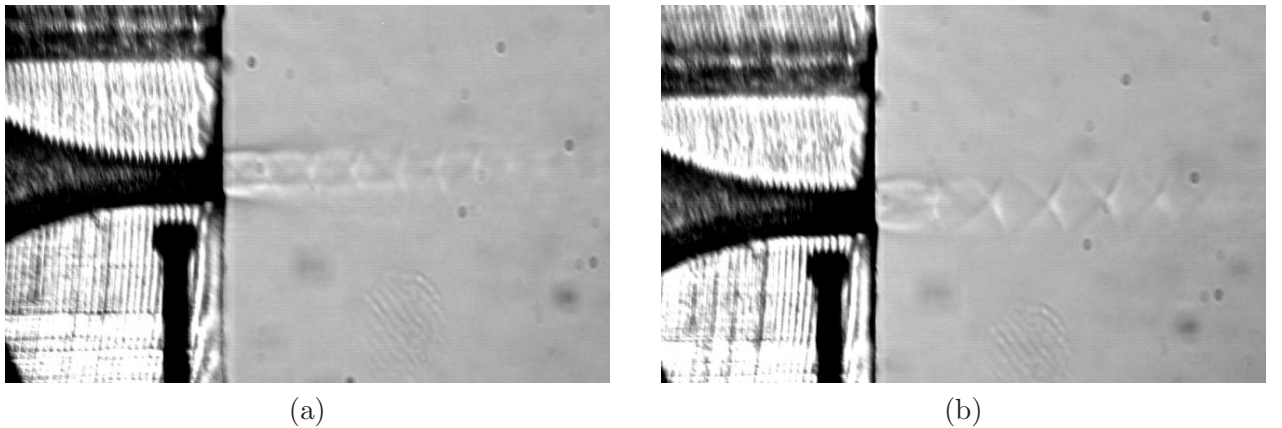| (a) | (b) |

Figure 24: Schlieren flow visualization images using (a) carbon dioxide and (b) air as the fluid.

to changes in the throat area relative to the exit Mach number. Future piezoelectric actuation is expected to provide novel, broadband flow control in a highly compact, supersonic actuator that can fit in a number of aircraft control surfaces where volume is a premium. A patent application has been submitted for review on this design.

5.2 Resonance Enhanced Actuator

Active control of high speed flow demands high amplitude and high-bandwidth actuation techniques for the effective and efficient manipulation of high energy and momentum flow structures that are often responsible for the adverse flow characteristics. The present studies focus on the development, design, and characterization of a novel high-bandwidth microactuator that can generate high frequency pulsed microjets over a large bandwidth and its implementation to various high and low-speed flow control applications. This micro fluidic actuator essentially consists of a primary under expanded source jet incident upon a cylindrical cavity with micro orifices at the bottom surfaces, through which the pulsed microjets flow out (Figure 25)(a). The microschlieren image of actuator flowfield is shown in Figure 25(b).

The main parameters that govern the flow properties of the microjet array issuing from the actuator assembly are: a) the distance from the source jet h, b) the length of the cylindrical cavity, L and c) the source jet pressure ratio, NPR. Experiments were conducted over a wide range in terms of geometric and flow parameters, where h/d is varied from 1 to 2, L/d from 1 to 5 and NPR from 1.9 to 6.3. The objective was to examine and understand the effect of these parameters on the flowfield issuing from the actuator array and to identify the optimal range and combination of these parameters that produce the desired microactuator flow such that smart structures can be integrated into the next generation design. Furthermore, we aim to develop a preliminary design approach and scaling laws for such actuators. The typical pressure spectra of pulsing microjets are shown in Figure 26. This corresponds to a case where L/d=2 and for variations in parameters NPR and h/d. As seen in Figure 26, for $L/d = 2$, an h/d variation from 1.0 to 1.5 has resulted in a frequency response of 36 to 24 kHz with discrete frequency amplitudes of 162 dB and 150 dB, respectively. Similarly, increasing the NPR from 4.4 to 5.5 (Figure 26(b)), shifts the frequency from 26 kHz to 34 kHz while increasing the peak amplitude by roughly 15 dB (see [14] for more details).

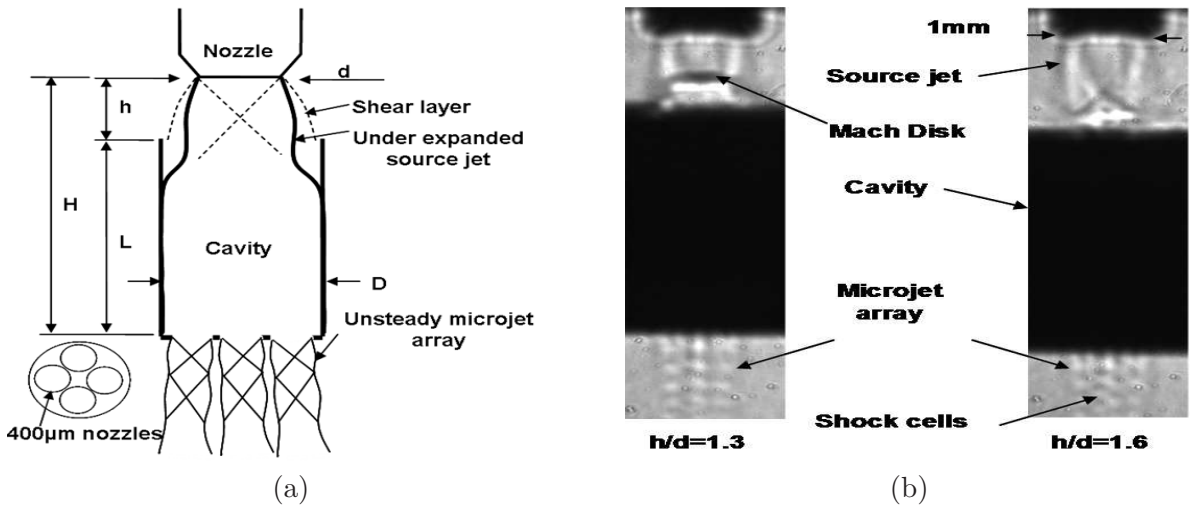Experiments were conducted over range of parametric combinations of $L/d, h/d$ and NPR. The

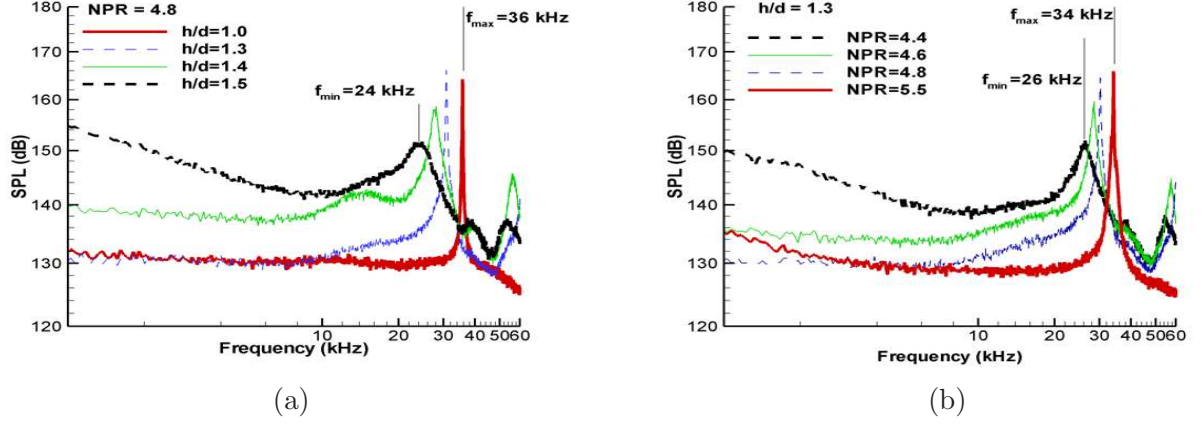Figure 25: (a) Schematic of microactuator. (b) Flowfield of microactuator

Figure 26: (a)Fixed NPR, h/d variation. (b) Fixed h/d, NPR variation.

non dimensional frequency of actuator is plotted against a new variable $H(H = L + h)$ as shown in Figure 27. The single trend curve shown in Figure 27 represents a correlation that can be used for the actuator design. The correlation is given by

$$St_{ideal} = 0.4 \left(\frac{H}{d} \right)^{-1.45}. \tag{5.1}$$

The results to date clearly show that the microjets produced by this actuator possess very high mean momentum (they are supersonic for most cases, velocity >300 m/s) as well as a very significant unsteady component (50-100 m/s). The ability to produce unsteady flow with significant mean and unsteady components, where the dynamic range can be easily varied makes these actuators promising for a number of high and low speed flow control applications. It should be noted that the internal aerodynamics within the cavity that occur during pulsed actuation cannot be easily visualized, as illustrated in Figure 25(b). Therefore, we conduct aero-acoustic computations to futher understand the fluid-structural interactions within the resonant cavity and its effect on the exit pulsed microjet flow.

5.2.1 Computational Correlations

For our computational study on resonance enhanced actuators, we considered the single-orifice actuator geometry depicted in Figure 28(a) in comparison to the multi-orifice design shown in Figure 25. Figure 28(b) shows the experimentally measured spectra of this actuator at various nozzle pressure ratios (NPR, which is the ratio of the source jet stagnation pressure to ambient pressure). It is clearly seen that, besides the actuator geometric parameters, the NPR is an important parameter that determines the frequency of the most energetic tone observed in the spectra, and its harmonics. For the present simulation test case, the NPR is set to 6.8. Source jet stagnation temperature is the same as the ambient temperature and equal to 68° Fahrenheit. This simulation test case corresponds to an experimentally studied case summarized in [14].

A general-purpose computational fluid dynamics methodology which allows the study of a wide range of fluid flow, turbulence and aeroacoustic problems of interest was utilized for the calculations. The simulation methodology has multi-block and overset grid capabilities, which provide flexibility in meshing complex computational domains while allowing grid density control in various regions of the flow domain. Optimized prefactored fourth-order accurate compact finite difference schemes [26]
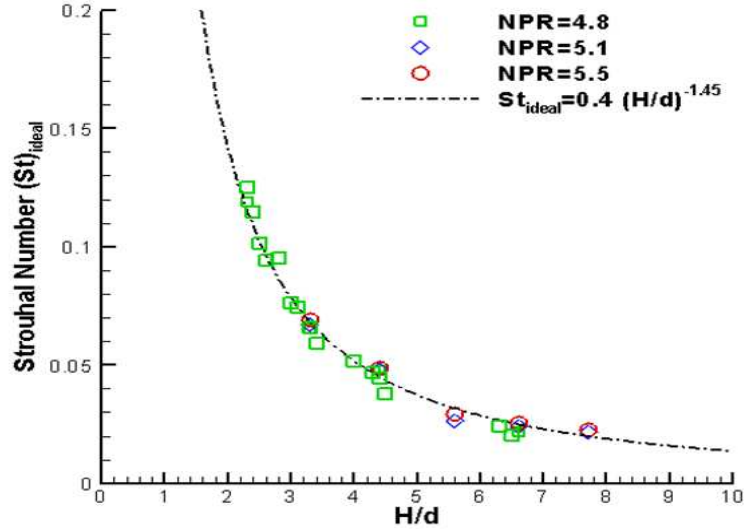
Figure 27: Design correlation for the actuator. The curve fit is based on (5.1).

and sixth-order accurate compact filters [27] ensure a high-quality numerical solution for multi-scale, multi-physics problems while temporally second-order accurate implicit time stepping [28] brings great savings in computing cost for wall-bounded problems in particular. State-of-the-art nonreflecting boundary conditions are used for far-field and inflow/outflow boundaries [29,30], while characteristic-type boundary conditions are applied on solid walls [31]. Sixth-order accurate explicit Lagrangian interpolation is employed for data exchange between overset grids [32]. Shock capturing in supersonic flows is accomplished by means of artificial dissipation [33], which is only added in the vicinity of the shock-containing regions. A special shock detector identifies the shock regions in the flow and determines where to explicitly apply the artificial dissipation. No explicit turbulence modeling is employed for the sub-grid scales which are not resolved by the computational grid. The spatial filtering process adds numerical dissipation to damp out the very small scales which are not well resolved by the computational grid, thus the numerical dissipation provided by the filtering process is treated as an implicit sub-grid scale model. This approach belongs to the implicit large eddy simulation class of methods. More details of the simulation methodology can be found in Reference [34].

The computational setup exactly duplicates the actuator geometry. The total number of grid points used in the fully three-dimensional calculation is approximately 92 million. The simulation has been performed on 720 processors running in parallel. The Reynolds number based on the ambient sound speed, ambient fluid kinematic viscosity and source jet nozzle inner diameter is roughly 23,000. The computational grid used for the simulation of the highly unsteady actuator flow field is expected to directly resolve the most energetic length scales of turbulence, thus the present simulation can be considered as a quasi direct numerical simulation. The simulation time step corresponds to about 7.3 nanoseconds.

Figures 29, 30 and 31 depict the instantaneous snapshots of the simulated actuator flow field in terms of density contours on a two-dimensional plane during the various stages of the cavity fill-and-discharge cycle and make qualitative comparisons with the corresponding experimental micro-Schlieren images. We divide one periodic cycle into 12 equally spaced snapshots. The phase difference between two successive snapshots is $30°$. The colored figures denote the simulation results, while the gray scale images correspond to the experimental measurements. There is very good overall

(a) Actuator schematic.
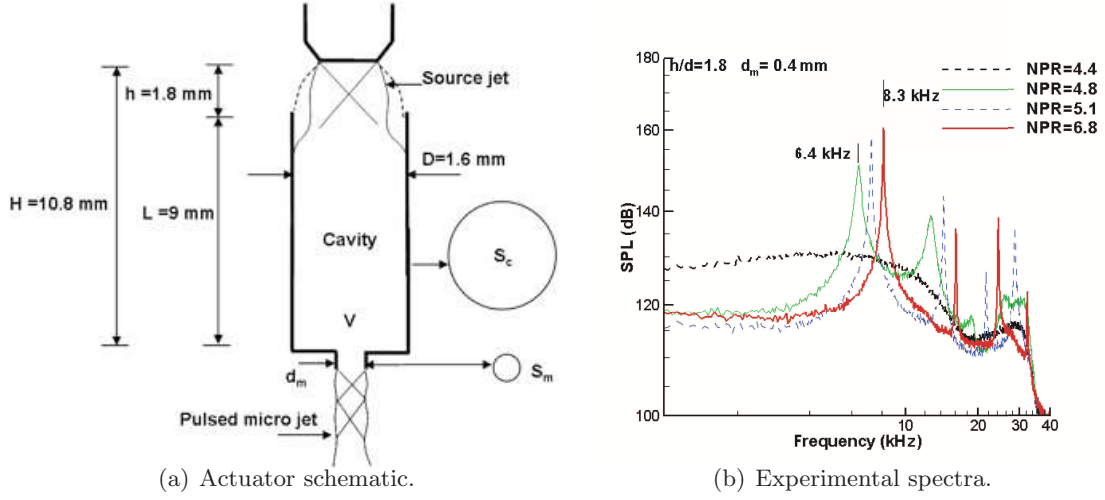
(b) Experimental spectra.

Figure 28: Geometric details of the single-orifice actuator geometry considered in the numerical simulation and the corresponding experimentally measured spectra of the pulsed microjet at various nozzle pressure ratio (NPR) values.

qualitative agreement between the simulation predicted flow field and experimental measurements. Although the flow within the cavity cannot be visualized in the experiment, it is seen that the details of the flow field in the region between the source jet exit and the cavity entrance show remarkable similarity between the simulation and experiment. Good similarity is also observed in the comparison of the microjet structure.

The high NPR results in an under-expanded jet issuing from the source jet nozzle. This under-expanded source jet results in a Mach disk which forms at some distance above the cylindrical cavity entrance. During the cavity fill stage, which is visualized by the snapshots at the phase angles of 180° through 270°, the Mach disk above the cavity helps guide much of the source jet flow towards the cavity volume. Once the cavity is completely filled up by the source jet, there is enough pressure build up inside the cavity to push the Mach disk away from the cavity entrance. The snapshot at the phase angle of 300° roughly marks the end of the cavity fill stage and the beginning of the discharge stage. Much of the source jet flow is directed outside the cavity while the Mach disk is displaced away from the cavity entrance. It is observed that part of the flow within the cavity spills out through the cavity entrance during the discharge stage. This spilled out flow from the cavity and the diverted source jet flow create a wall jet above the cavity during the discharge stage. The discharge stage is visualized by the snapshots at the phase angles of 330°, and 0° through 120°. The snapshot at the phase angle of 150° roughly marks the end of the discharge stage and the beginning of the fill stage.

It is observed that the microjet issuing through the orifice at the bottom of cavity has a strong resemblance to jets at much larger scale. The microjet is supersonic and contains shock cells during part of the cycle where the pressure at the bottom of the cavity is high enough with respect to the ambient pressure to create a supersonic flow through the orifice. Snapshots at the phase angles of 240° through 330° and also at 0° clearly depict the shock cell structure within the supersonic microjet. As the cavity discharges, the pressure at the bottom of the cavity eventually drops to near ambient levels, which is not strong enough to drive a supersonic flow through the orifice. This results in a relatively low-speed microjet through the orifice for the rest of the discharge stage. The snapshots at the phase angles of 0°, 30° and 60° show the transition of the microjet from supersonic

to subsonic state. The microjet continues to remain subsonic during the early part of the cavity fill stage, as can be seen at the phase angles of 150° and 180°, and becomes supersonic again once the pressure at the cavity bottom rises to a high enough level with respect to the ambient pressure. The snapshots at the phase angles of 180°, 210° and 240° show the transition of the microjet from subsonic to supersonic state.

Flow visualizations from the simulation show that one fill-and-discharge cycle of the cylindrical cavity takes place over roughly 120.8 microseconds, corresponding to a fundamental frequency of around 8.3 kHz. Measured experimental spectra show that the frequency of the most energetic tone is also 8.3 kHz for the given NPR, as can be seen in Figure 28(b). Thus, it is observed that there is excellent agreement between the experimentally measured fundamental frequency and the simulation predicted value.

Animations of the simulated actuator flow field can be viewed and downloaded at the following web address: http://www.math.fsu.edu/~auzun/SingleOrificeActuator/. These animations provide detailed visualizations of the pulsed actuator operation in terms of density, pressure, temperature and axial velocity contours. The detailed findings from this computational study can be found in an upcoming publication [35] which will be available in the near future.

6 Discussion and Concluding Remarks

This project has provided new, fundamental understanding of the limits of supersonic pulsed-mode microjet actuation for separation flow control and noise reduction problems. The combination of smart structure actuator design and modeling in combination with advanced flow diagnostics has provided new knowledge on these challenging flow control problems. A key to this effort was the combination of inter-disciplinary research between the PI who specialized in solid mechanics and actuator development of smart materials and structures and the co-PI who specialized in advanced aero-dynamic flow control actuators and flow visualization. In summary, the main focus of this project was to identify methods to achieve broadband pulsed flow control using piezohydraulic actuation. Over the course of the three year project, this led to new designs that improve reliability while reducing the volume, mass, and complexity of the pulsed flow actuator. Specific details regarding the technical achievements and challenges are given in the subsequent paragraphs.

A piezoelectric hydraulic actuator design has been applied to pulsed microjet flow problems to understand microscale flow dynamics over a broad frequency range. Sufficient hydraulic amplification, on the order of 65× the stack actuator displacement, has been utilized for throttling a 400 μm diameter microjet. Pulsed flow was achieved over a frequency of 1 kHz. Minimal attenuation of the microjet exit pressure response is observed up to 400 Hz. Moreover, there is less than a 40 % reduction in peak to peak pressure at 1 kHz compared to 1 Hz. Pulsed flow was also achieved up to a frequency of 1.6 kHz. At a pulsing microjet flow frequency of 1.6 kHz, there was a ∼60 % reduction in performance compared to base line tests at 1 Hz. Little attenuation in overall performance is also evident from the power spectral density for this broadband frequency range.

A comparison of *in situ* stack actuator displacements and pressure measurements were taken to quantify and correlate the internal dynamic characteristics of the stack actuator versus exit dynamic pressure as a function of the applied electric field to the stack actuator. This data provided more insight into the internal dynamics relative to the output pressure. A noticeable phase angle offset between the input voltage to the piezoelectric stack actuator and exit flow pressure is present as the input frequency increases. However, once uncertainty in monitoring the displacement of the piezoelectric stack during pulsed flow tests is reduced, feedback control methods can be used to increase system performance attributes and reduce the lag between system components. It is believed

(a) Phase angle = 0°

(b) Phase angle = 30°

(c) Phase angle = 60°

(d) Phase angle = 90°

Figure 29: Side-by-side qualitative comparison of simulation result with experimental measurement at phase angles of 0° through 90°.

(a) Phase angle = 120°

(b) Phase angle = 150°

(c) Phase angle = 180°

(d) Phase angle = 210°

Figure 30: Side-by-side qualitative comparison of simulation result with experimental measurement at phase angles of 120° through 210°.

(a) Phase angle = 240°

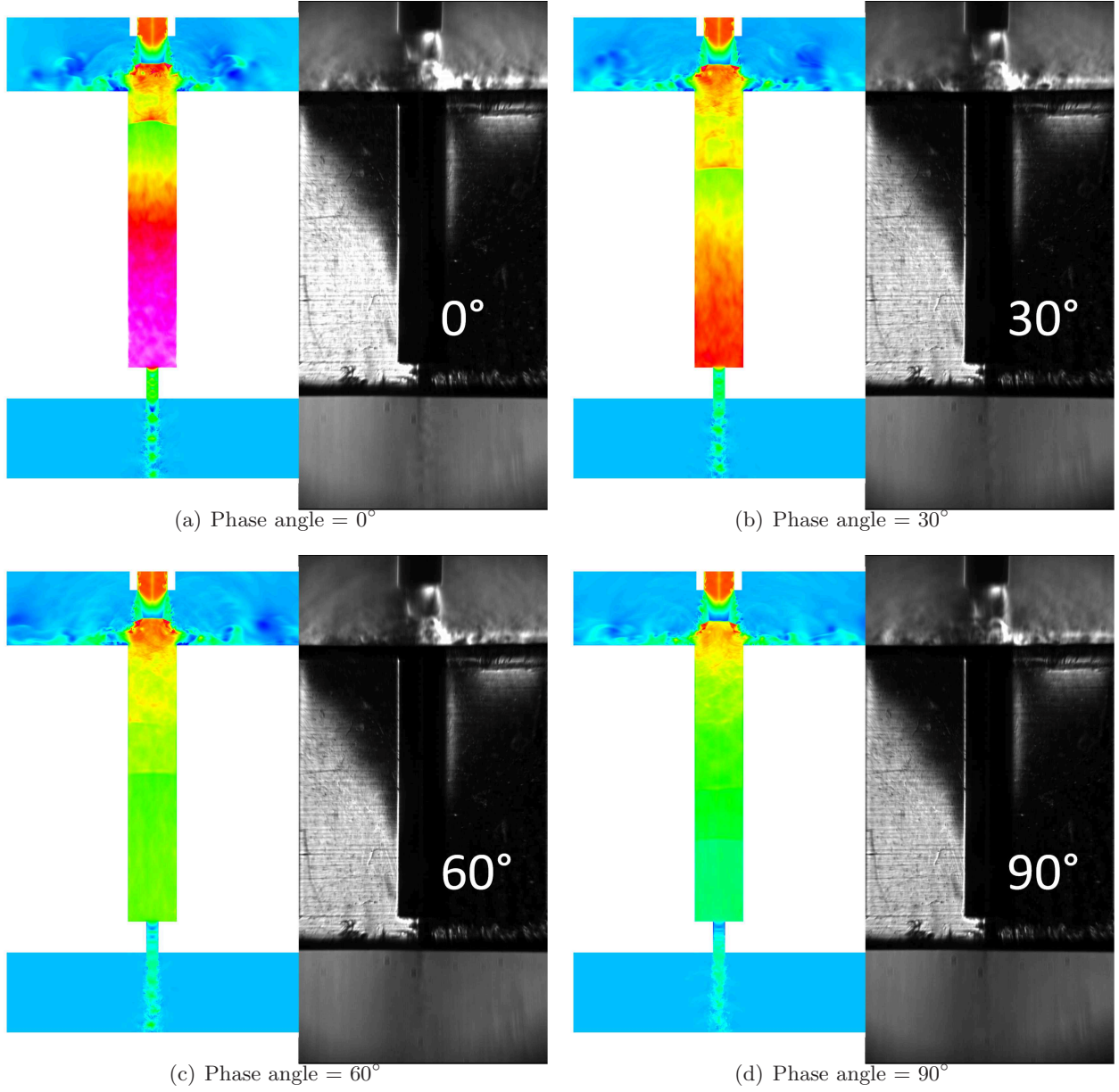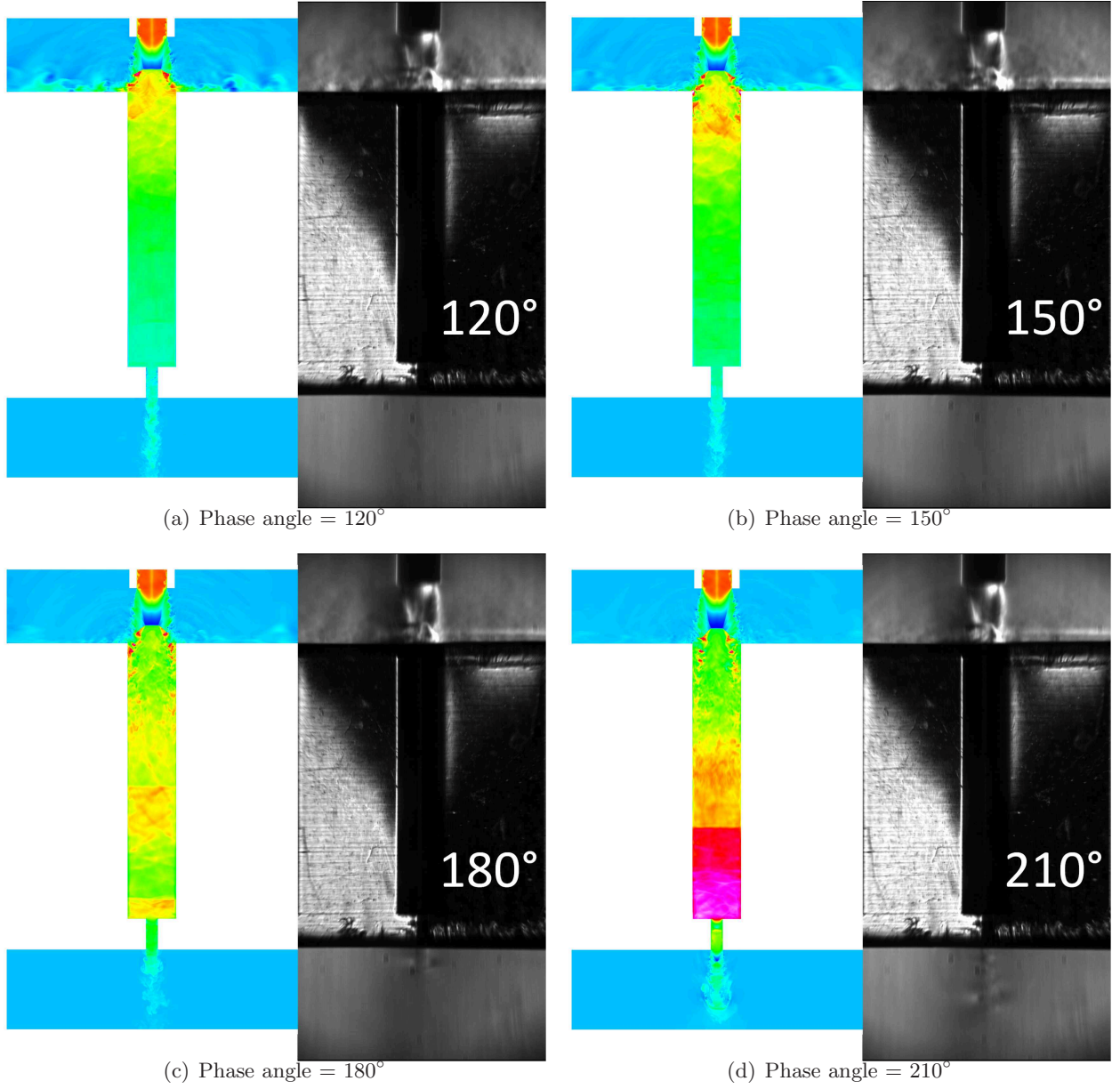(b) Phase angle = 270°
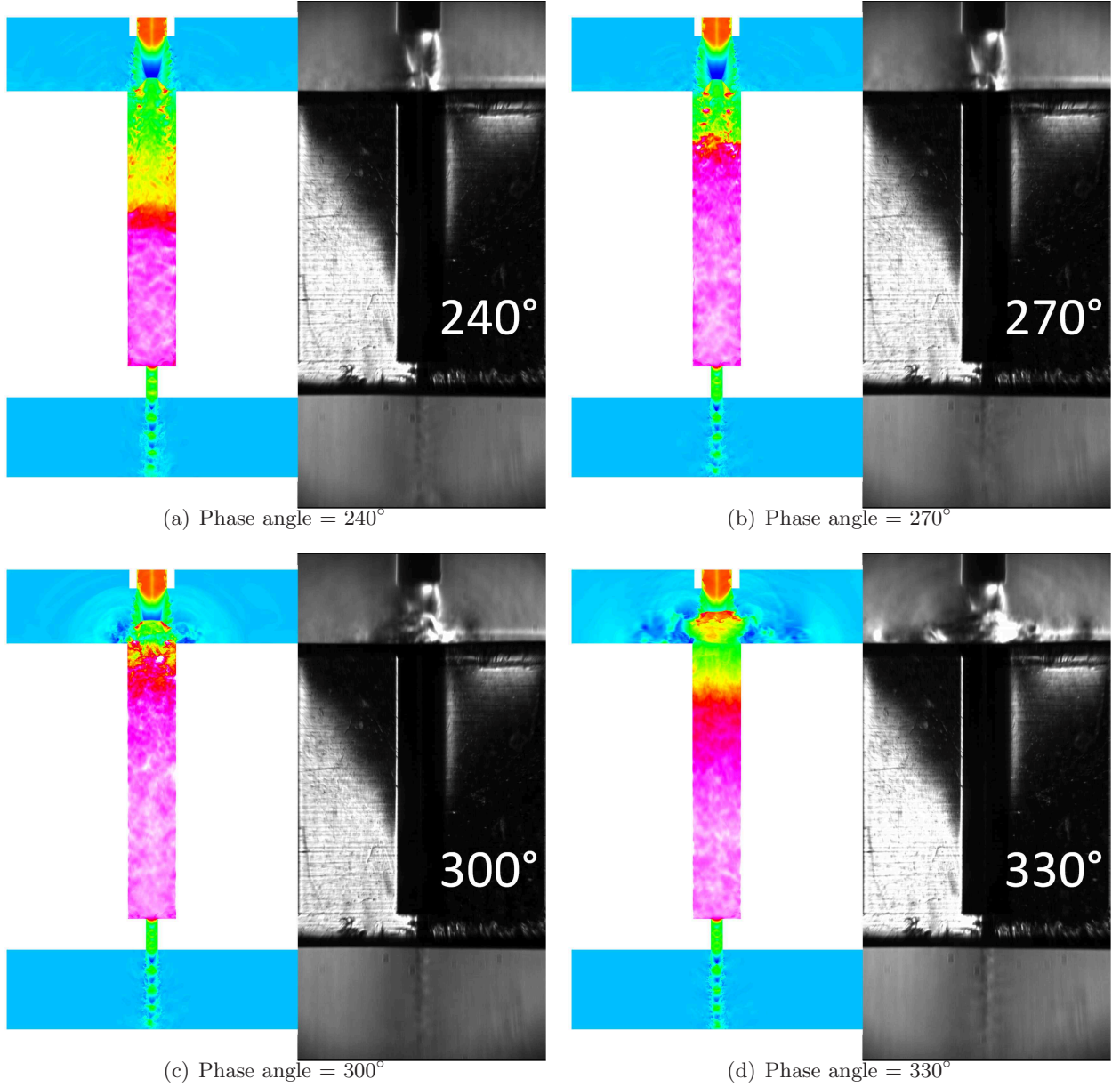
(c) Phase angle = 300°

(d) Phase angle = 330°

Figure 31: Side-by-side qualitative comparison of simulation result with experimental measurement at phase angles of 240° through 330°.

that placing the strain gauge underneath the epoxy layer of the piezoelectric stack actuator will reduce uncertainty in the strain gauge measurements. Additional phase lags between input voltage and pressure response may be attributed to the rate dependent ferroelectric behavior of the piezoelectric stack actuator, nonlinearities of the rubber diaphragm, and the fluid inertia in the cylinder head.

Micro-Schlieren measurements were also conducted to correlate dynamic pressure with flow visualization on the piezohydraulic actuator. The sonic nozzle demonstrated the formation of shock cells as the piezohydraulic valve was throttled from fully open to fully closed. This was found to occur up to 800 Hz. Whereas attenuation becomes apparent at this higher frequency, large changes in the Mach number are still achieved as indicated by shock cells in Figure 21. This validates the pressure data collected and the performance characteristics noted up to 800 Hz.

The results are promising for establishing fundamental pulsed flow interactions with a non-zero external flow field to understand how the microjet amplitude, frequency, and phase affects a number of flow control problems. Current work focused on establishing these interactions under ambient conditions. Future opportunities exist to understand how these pulsed flow characteristics influence external flow fields. Particle image velocimetry experiments should be conducted to obtain quantified performance metrics. In addition, rate dependent nonlinearities of the ferroelectric material may affect microjet interactions with the external flow field. Since these effects are amplified through the hydraulic circuit, large nonlinear and hysteretic pressure versus electric field responses can occur. This introduces higher order harmonics. However, by eliminating the hydraulic fluid using the A* actuator (Section 5.1) these affects may be mitigated. The system dynamic model established in [36] also provided key insight into the nonlinear coupling behavior within the microjet device which isolated amplification of hysteresis through the hydraulic amplification. It also was instrumental in identifying how snap-through buckling lead to large displacment amplification and how this behavior could be achieved at relatively large frequencies (up to 1 kHz).

The section on next generation adaptive structure microjet actuators has provided a route towards embedding these broadband actuators within confined aerodynamic structures for flow control applications such as dynamic stall on rotorblades and noise reduction. Further work is recommened to:

1. Quantify performance trade-offs between the next generation actuators and the piezohydraulic actuator under different external flow conditions and aerodynamic surfaces.

2. Quantify the pulsed jet pressure amplitude, frequency and phase on flow separation and noise reduction problems. This should include PIV measurements which could be conducted under sub-sonic, trans-sonic, and supersonic at the new polysonic wind tunnel currently under development at Florida State University within the Florida Center for Advanced Aero-Propulsion (FCAAP).

3. Identify ideal active (piezoelectric) actuators that can operate over a broad temperature, voltage, and input voltage frequency range. For example, ferroelectric relaxors such as PMN-PT or PZN-PT are more stable in terms of electro-mechanical properties over a broader temperature and frequency range relative to PZT (lead zirconate titanate) which may provide robustness in harsh environments.

References

[1] A. L. Braslow, "A history of suction-type laminar-flow control with empahsis on flight research," *NASA Monographs in Aerospace History*, no. 13, 1999.

[2] D. Greenblatt and I. Wygnanski, "The control of separation flow by periodic excitation," *Prog. Aerosp. Sci.*, vol. 36, pp. 487–545, 2000.

[3] D. G. M. David R. Williams, "Brief history of flow control," *Chapter 1. Fundamentals and Applications of Modern Flow Control, Edited by R. Joslin and D. Miller*, vol. 231, pp. 1–20, 2009.

[4] N. M. McFadden, G. A. Rathert, and R. S. Bray, "The effectiveness of wing vortex generators in improving maneuvering characteristics of a swept wing airplane at transonic speeds," *NACA*, no. TN-3523, 1955.

[5] D. W. Bechert, M. Bruse, W. Hage, J. VanDerHoeven, and G. Hoppe, "Experiments on drag-reducing surfaces and their optimization with an adjustable geometry," *J. Fluid Mech.*, vol. 338, pp. 59–87, 1997.

[6] R. L. Clark, "Evaluation of f-111 weapon bay aero-acoustic and weapon separation improvement techniques," no. AFFDL TR-79-3003, 1979.

[7] L. Cattafesta, D. Williams, C. Rowley, and F. Alvi, "Review of active control of flow-induced cavity resonance," *AIAA Paper 03-3567*, no. 3567, June 2003.

[8] B. Henderson, J. Bridges, and M. Wernet, "An experimental study of the oscillatory flow structure of tone-producing supersonic impinging jets," *J. Fluid Mech.*, vol. 524, pp. 115–137, 2005.

[9] F. Alvi, C. Shi, R. Elavarasan, G. Garg, and A. Krothapalli, "Control of supersonic impinging jet flows using supersonic microjets," *AIAA Jrnl.*, vol. 41, no. 7, pp. 1347–1355, 2003.

[10] R. Kumar, S. Lazic, and F. S. Alvi, "Active control of high temperature supersonic impinging jets," *AIAA*, no. 360, 2008.

[11] K. R. Grossman, B. Z. Cybyk, M. C. Rigling, and D. M. VanWie, "Characterization of sparkjet atuators for flow control," *AIAA*, vol. 42, no. 89, 2004.

[12] A. Glezer and M. Amitay, "Synthetic jets," *Annu. Rev. Fluid Mech.*, vol. 34, pp. 503–529, 2002.

[13] L. Cattafesta, S. Garg, M. Chourdhari, and F. Li, "Active control of flow-induced cavity resonance," *AIAA Paper 97-1804*, 1997.

[14] J. T. Solomon, R. Kumar, and F. Alvi, "High bandwidth pulsed microactuators for high speed flow control," *AIAA*, vol. 48, no. 10, pp. 2386–2396, 2010.

[15] B. Jaffe, W. Cook, and H. Jaffe, *Piezoelectric Ceramics*. London: Academic Press, 1971.

[16] J. M. Wiltse and A. Glezer, "Manipulation of free shear flows using piezoelectric actuators," *Journal of Fluid Mechanics*, vol. 249, pp. 261–285, 1993.

[17] A. Seifert, S. Eliahu, D. Greenblatt, and I. Wygnanski, "Use of piezoeletric actuators for airfoil separation control," *AIAA*, vol. 35, no. 8, pp. 1535–1536, 1998.

[18] V. Kumar and F. Alvi, "Use of high-speed microjets for active separation control in diffusers," *AIAA Jrnl.*, vol. 44, no. 2, pp. 273–281, 2006.

[19] W. Oates and C. Lynch, "Piezoelectric hydraulic pump system dynamic model," *J. Intell. Mater. Syst. Struct.*, vol. 12, no. 11, pp. 737–744, 2001.

[20] W. Oates and F. Liu, "Piezohydraylic actuator devleopment for microjet flow control," *J. Mech. Des.*, vol. 131, no. 9, p. 091001 (9 pages), 2009.

[21] R. Smith, *Smart Material Systems: Model Development.* Philadelphia, PA: SIAM, 2005.

[22] F. Liu, J. Hogue, W. Oates, J. Solomon, and F. Alvi, "Piezoelectric controlled pulsed microjet actuation," *SMASIS*, no. 1448, 2009.

[23] K. A. Phalnikar, R. Kumar, and F. S. Alvi, "Experiments on free and impinging supersonic microjets," *Exp Fluids*, vol. 44, pp. 819–830, 2008.

[24] J. Hogue, *Broadband microjet flow control using piezoelectric actuators.* Florida State University: M.S. Thesis, 2011.

[25] J. Hogue, M. Brosche, W. Oates, and J. Clark, "Development of a piezoelectric supersonic microactuator for broadband flow control," *Proc. Florida Center of Advanced Aero Propulsion (FCAAP) Conference, Orlando, FL, August 2009*, 2009. [Online]. Available: http://www.eng.fsu.edu/~woates/

[26] G. Ashcroft and X. Zhang, "Optimized prefactored compact schemes," *Journal of Computational Physics*, vol. 190, no. 2, pp. 459–457, 2003.

[27] D. V. Gaitonde and M. R. Visbal, "Padé-type higher-order boundary filters for the Navier-Stokes equations," *AIAA Journal*, vol. 38, no. 11, pp. 2103–2112, November 2000.

[28] J. A. Ekaterinaris, "Implicit, high-resolution, compact schemes for gas dynamics and aeroacoustics," *Journal of Computational Physics*, vol. 156, no. 2, pp. 272–299, 1999.

[29] J. W. Kim and D. J. Lee, "Generalized characteristic boundary conditions for computational aeroacoustics," *AIAA Journal*, vol. 38, no. 11, pp. 2040–2049, November 2000.

[30] T. Z. Dong, "On boundary conditions for acoustic computations in non-uniform mean flows," *Journal of Computational Acoustics*, vol. 5, no. 3, pp. 297–315, 1997.

[31] J. W. Kim and D. J. Lee, "Generalized characteristic boundary conditions for computational aeroacoustics, part 2," *AIAA Journal*, vol. 42, no. 1, pp. 47–55, January 2004.

[32] S. E. Sherer and J. N. Scott, "High-order compact finite-difference methods on general overset grids," *Journal of Computational Physics*, vol. 210, no. 2, pp. 459–496, December 2005.

[33] J. W. Kim and D. J. Lee, "Adaptive nonlinear artificial dissipation model for computational aeroacoustics," *AIAA Journal*, vol. 39, no. 5, pp. 810–818, May 2001.

[34] A. Uzun and M. Y. Hussaini, "Simulation of noise generation in near-nozzle region of a chevron nozzle jet," *AIAA Journal*, vol. 47, no. 8, pp. 1793–1810, 2009.

[35] A. Uzun, J. Solomon, C. Foster, W. Oates, M. Y. Hussaini, and F. Alvi, "Simulations of pulsed actuators for high-speed flow control," *Proceedings of the 17th AIAA/CEAS Aeroacoustics Conference, Portland, Oregon*, June 2011.

[36] W. Oates and F. Liu, "Piezohydraulic actuator development for microjet flow control," *J. Mech. Des.*, vol. 131, no. 9, pp. 091 001–091 010, 2009.

[37] J. Hogue, M. Brosche, W. Oates, and J. Clark, "Development of a piezoelectric supersonic microactuator for broadband flow control," *Proc. FCAAP: Florida Center for Advanced Aero Propulsion Conference*, August 2009.